Available online at www.sciencedirect.com
ScienceDirect
International Journal of Plasticity 24 (2008) 1549–1580
INTERNATIONAL JOURNAL OF Plasticity
www.elsevier.com/locate/ijplas

Multi-laminate plastic-strain organization for non-uniform TFA modeling of poly-crystal regularized plastic flow

P. Franciosi [a], S. Berbenni [b,*]

[a] LPMTM, UPR CNRS 9001, Institut Galilée, University of Paris 13, 93430 Villetaneuse, France
[b] LPMM, UMR CNRS 7554, ENSAM, Technopole, 57078 Metz Cedex 03, France

Received 16 March 2007; received in final revised form 19 November 2007
Available online 6 February 2008

Abstract

A recently presented single plastic-potential, microstructure-based model of poly-crystal plasticity by the authors considers a globally regularized Schmid law (RSL) as the slip flow criterion of a homogeneous equivalent super-crystal. The homogenization scheme that is taken of affine type is specialized to the transformation field analysis (TFA) framework. The relevancy of the TFA here results from a description of intra-crystalline slip in terms of hierarchical multi-laminate (HML) structures that ensure the request of piece-wise homogeneous plasticity. This RSL–TFA–HML modeling has been shown efficient for heterogeneous intra-crystalline plastic slip in terms of overall stiffness estimates when laminates are parallel to slip planes or normal to slip directions. It is also suitable for twinning modes of crystal plasticity as stressed in this paper. The performed superposition of all possible HML plastic strain modes makes the TFA of the non-uniform (NTFA) and coupled type proposed by Michel and Suquet [Michel, J.C., Suquet, P., 2003. Non-uniform transformation field analysis. International Journal of Solids and Structures 40, 6937–6955; Michel, J.C., Suquet, P., 2004. Computational analysis of nonlinear composite structures using the non-uniform transformation field analysis. Computer Methods in Applied Mechanics and Engineering 193, 5477–5502]. In this new contribution, we investigate further our extension of this modeling to poly-crystals. It is interpreted as based on a description of the aggregate morphology in terms of the distribution of the crystallographic orientations of the grain boundary and sub-boundary facets, rather than in terms of a mean grain or domain shape. In its initial form, our extension amounted to assuming all these facets oriented either parallel to slip planes or normal to slip directions, what is proved convenient for large enough grains. In order to extend the relevancy of the modeling down to ultra-

* Corresponding author. Tel.: +33 3 8737 5430; fax: +33 3 8737 4284.
E-mail address: Stephane.Berbenni@metz.ensam.fr (S. Berbenni).

0749-6419/$ - see front matter
doi:10.1016/j.ijplas.2007.12.004

fine grains, we introduce a graded form of the modeling that is made grain size dependent from specifying the conditions for which the TFA accommodation hardening is negligible according to the range of the physical one. Some numerical stiffness comparisons from this graded RSL–TFA–HML modeling are provided.

Keywords: A. Multi-laminate structures; B. Crystal plasticity; B. Polycrystalline material; B. Ultrafine-grained material; C. Homogenization

1. Introduction

In order to describe the plastic flow of single crystals under the rate-independent hypothesis, a regularized form of the Schmid law for slip has been proposed (Arminjon, 1991; Gambin, 1991, 1992; Imbault and Arminjon, 1998). This description was introduced to eliminate the Schmid law singularities on the crystal yield surface and to consequently suppress the related solution uniqueness problem (Franciosi and Zaoui, 1991). Such a single plastic-potential, microstructure-based model provides obvious advantages in theoretical and computational modeling, as for instance in finite element codes devoted to metal forming simulations. This is the reason why the extension of this regularized Schmid law (RSL) from single crystal to poly-crystal plastic flow has been considered by different authors (Darrieulat and Piot, 1996; Kowalczyk and Gambin, 2004), but mostly under the severe assumptions of stress or of strain uniformity.

This extension has been reconsidered in Berbenni and Franciosi (2004) and Franciosi and Berbenni (2007) within a more general homogenization framework of the affine type (Ponte-Castaneda and Suquet, 1998; Masson et al., 2000) which enables to satisfactorily account for both stress and strain heterogeneities from grain to grain as well as in the grains. A difference with earlier works is that the RSL is globally applied to a homogeneous equivalent super-crystal of the aggregate. In counterpart to this introduced new complexity, the required conditions to make use of the transformation field analysis (TFA) framework (Dvorak, 1992; Dvorak and Benveniste, 1992) have been fulfilled. Namely, the prerequisite of a partition of the material into plastically homogeneous domains (Suquet, 1997; Chaboche et al., 2001) has been satisfied by assuming that intra-crystalline slip arranges into multi-laminate structures, in which the layers have "almost everywhere" uniform strain and stress fields. However, relevant and manageable arrangements of slip remained to be proposed.

Many theoretical works have been devoted to multi-laminate structures in various elastic or elastic–plastic contexts (see Francfort and Murat, 1986; Quintanilla and Torquato, 1996; El Omri et al., 2000; Debotton and Hariton, 2002). In the particular context of crystal plasticity, Ortiz and Repetto (1999) show how multi-laminate descriptions rapidly face complexity for restituting the corresponding microstructural evolutions. In comparison, the main interest of the proposed RSL–TFA–HML modeling, with "HML" standing for "Hierarchical-Multi-Laminate", is based on an orthogonality property that has been pointed out in Franciosi and Berbenni (2007): for laminate layers that are taken parallel to one slip plane orientation, the corresponding contributions to the TFA-due over-stiffness cancel.

This property results from the relative expressions of the modified Green operator integral associated to one laminate orientation and of the Schmid tensors of the slip systems whose slip plane is parallel to the laminate layers. Hence, a slip organization which

assumes successive laminate orientations to be parallel to those of the P slip planes of the considered crystal lattice yields rank-$(P-1)$ laminate structures, here called $(P-1)$-HML structures. The number of possible $(P-1)$-HML structures for a given set P of slip planes is the number $P!$ of their permutations. The superposition of these $P!$ slip arrangements, weighted by their respective occurrence probabilities, yields an effective crystal plastic behavior with no or negligible TFA-due over-stiffness. This weighted superposition of possible plastic "modes" makes the TFA modeling with HML structures for slip to be of the non-uniform (NTFA) and coupled type that has been proposed by Michel and Suquet (2003, 2004). They proved that this type of modeling yields accurate estimates of overall behavior in nonlinear heterogeneous plasticity, provided the identification of appropriate elementary modes to be coupled and superimposed. This is what has been done here, with a physically based introduction of such modes at the slip system scale.

Beyond the objective to derive a suitable heterogeneous description of crystal plasticity in the TFA framework, the introduction of HML structures to describe crystallographic slip enabled as expected an extension of the proposed modeling to poly-crystals, through their homogeneous equivalent super-crystal. This extension has been introduced by simple analogy with the heterogeneous crystal case in Franciosi and Berbenni (2007) where it was pointed out that the modified Green operator integral representative of a poly-crystal grain was similar, in discrete forms of its so-called polar decomposition, to the one of a HML structure.

But this analogy does not hold for an interpretation and the main purpose of the present paper is to investigate further the extension of this RSL–TFA–HML modeling to poly-crystal in terms of physical interpretation and relevancy. In Section 2, we briefly recall the constitutive equations of the RSL–TFA framework. Section 3 summarizes the characteristics of the HML description of slip organization and the conditions for which contributions to the TFA-due over-stiffness can be cancelled, including the consideration of possible twinning shear modes. The application of the RSL–TFA–HML modeling to poly-crystals is addressed in Section 4. An interpretation is given in terms of the distribution of the crystallographic orientations of the facets that constitute the grain boundaries and sub-boundaries down to the cell structure. From this viewpoint, the RSL–TFA–HML modeling amounts to assuming all these facets oriented either parallel to slip planes or normal to slip directions. This interpretation appearing convenient for large enough grains but quite excessive for small ones, special attention is paid to the conditions for which the TFA accommodation hardening is negligible according to the range of the physical hardening. This leads us to propose a "graded" RSL–TFA–HML modeling that is made grain size dependent and consistent with the proposed interpretation down to ultra-fine grained poly-crystals. Some numerical simulations that illustrate the capabilities of this modeling are reported in Section 5.

2. The TFA framework applied to a regularized poly-crystal plasticity modeling

We consider homogeneous crystalline domains in which plastic flow results from crystallographic glide on N slip systems defined by a pair of orthogonal unit vectors $\mathbf{n}^g$ and $\mathbf{m}^g$, respectively normal to the slip plane and parallel to the slip direction. In the simplest case, all N slip systems and therefore all P slip planes are crystallographically identical with same $p = N/P$ sets of coplanar systems on them. For example, $P = 4$ and $p = 3$ in FCC structures with (1 1 1) slip planes and $<1\,1\,0>$ slip directions, and $P = 6$, $p = 2$ in BCC

crystals when slip is restricted to the (1 1 0) planes and to the ⟨1 1 1⟩ directions. More generally, several types t of slip systems coexist, for $N^{(t)} = \sum_{i=1}^{t} N^i$ systems, corresponding to different (P^i, p^i), $i \in (1, t)$ plane and coplanar system numbers (for example the association of basal, prismatic and pyramidal slip in HCP crystals, or slip on (1 1 0) and on other (1 x−1 x) planes, with $x = 2, 3, \ldots$) planes, with $x = 2, 3, \ldots$) for BCC crystals. All the system types are therefore defined by a pair $(\mathbf{n}^{g(t)}, \mathbf{m}^{g(t)})$ of orthogonal unit vectors, but the superscript "t" will be omitted in the following.

Generally, real crystals are imperfect because they are not totally free from lattice disorientations which are either grown (mosaic) or to plastic strain due. A homogeneous equivalent medium for an imperfect crystal would be a super-crystal of same volume V that superimposes at every point all the slip systems $g(I)$ of all perfect sub-domains I of V, as far as they are countable. Like imperfectly grown (mosaic) crystals, grown polycrystalline aggregates are spatial assemblages of disoriented grain-like perfect domains but with broader distributions of disorientations between them. When intra-crystalline heterogeneities result from heterogeneous plastic strain history, the self-organization of the sub-domains becomes more complex. The accessible characteristics are orientation or disorientation distributions of the domains and orientation distribution of their boundaries. Pole figures or orientation distribution functions allow to defining a homogeneous equivalent super-crystal for imperfect crystals and for any poly-crystal as well. In the poly-crystal case, the super-lattice is defined by its crystallographic texture.

For any perfect crystalline domain I in imperfect crystals as well as in poly-crystals, we introduce the slip system Schmid tensors defined by $\mathbf{R}^{g(I)} = \{\mathbf{m}^{g(I)} \otimes \mathbf{n}^{g(I)}\} = \mathbf{R}^{tg(I)}$, with "{}" standing for "symmetric part of", and $\mathbf{R}^t$ for the transpose of $\mathbf{R}$. Thus, perfect lattice domains are characterized by uniform Schmid tensors for all slip systems. It is noteworthy that the twinning modes of plastic straining that may be involved with slip in crystal plasticity are also crystallographically characterized by a pair $(\mathbf{n}^g, \mathbf{m}^g)$ of orthogonal unit vectors and a Schmid tensor $\mathbf{R}^g = \{\mathbf{m}^g \otimes \mathbf{n}^g\}$.

In the following, the mean (volume average) of $x(\mathbf{r})$ in R^3 is denoted $\bar{x} = \frac{1}{V}\int_V x(\mathbf{r})d\mathbf{r}$ and T, $g = \partial T/\partial g$. The following Sections 2.1 and 2.2 briefly present the considered extension to poly-crystal plasticity of the regularized Schmid law respectively in a general affine formulation and in the TFA framework. This formalism has been introduced by Franciosi and Berbenni (2007) at first for the case of heterogeneous intra-crystalline slip. Specific features that would concern twinning modes whenever some may contribute are addressed in Section 2.3.

2.1. The extension to poly-crystals of the regularized Schmid law (RSL) as plastic flow criterion

When the regularized Schmid law (RSL) is globally applied to the homogeneous equivalent super-crystal of an aggregate, the heterogeneities of plastic behavior are accounted for through the chosen homogenization/localization scheme. Let us a priori consider aggregates of possibly heterogeneous grains with an interior morphology not necessarily similar to the aggregate one. In this case the global single plastic potential F that is given by the RSL can be written under the form:

$$F = \left(\left(\sum_I f_I \left[\sum_{\alpha(I)} f_{\alpha(I)} \sum_{g(\alpha(I))} \left(\frac{\tau^{g(\alpha(I))}}{\tau_c^{g(\alpha(I))}} \right)^n \right] \right)^{\frac{1}{n}} - 1 \right) \tau_{\mathrm{cref}} = F_0 \tau_{\mathrm{cref}} = 0. \tag{1}$$

In Eq. (1), if "I" represents a sum over grains in concentration f_I and if the interior summation over $g(\alpha(I))$ runs over a slip system set, the intermediate sum over $\alpha(I)$ can stand for different descriptions of grain partition or of intra-crystalline heterogeneous plasticity, as the proposed HML description of intra-crystalline slip. If these intra-crystalline heterogeneities of slip are disregarded, Eq. (1) can be considered as adapted to the possibility of twinning in the grains, with $\alpha(I)$ standing for twinned sub-domains in domain I.

Whatever the specific morphologies of these two levels of heterogeneity are, we consider an affine approximation for the homogenization of the nonlinear behavior of the aggregate of concern (Masson et al., 2000). Disregarding specific features of finite rate-independent crystal plasticity (Mc Ginty and Mc Dowell, 2006), the stress $\underset{\sim}{\boldsymbol{\sigma}}^{\alpha(I)}$ in the sub-domain $\alpha(I)$ can be written as

$$\underset{\sim}{\boldsymbol{\sigma}}^{\alpha(I)} = \underset{\approx}{\mathbf{B}}_*^{\alpha(I)} : \left(\underset{\approx}{\mathbf{B}}_*^{I} : \underset{\sim}{\boldsymbol{\Sigma}} + \sum_J \underset{\approx}{\mathbf{F}}_*^{IJ} : \widehat{\underset{\sim}{\boldsymbol{\varepsilon}}}^{*J} \right) + \sum_{\beta(I)} \underset{\approx}{\mathbf{F}}_*^{\alpha(I)\beta(I)} : \underset{\sim}{\boldsymbol{\varepsilon}}^{*\beta(I)} = \underset{\approx}{\mathbf{B}}_*^{\alpha_I} : \underset{\sim}{\boldsymbol{\Sigma}} + \sum_{\beta_J} \underset{\approx}{\mathbf{F}}_*^{\alpha_I\beta_J} : \underset{\sim}{\boldsymbol{\varepsilon}}^{*\beta_J} = \underset{\sim}{\boldsymbol{\sigma}}^{\alpha_I}, \tag{2}$$

with $\underset{\sim}{\boldsymbol{\sigma}}^{I} = \underset{\approx}{\mathbf{B}}_*^{I} : \underset{\sim}{\boldsymbol{\Sigma}} + \sum_J f_J \underline{\underset{\approx}{\mathbf{F}}}_*^{IJ} : \widehat{\underset{\sim}{\boldsymbol{\varepsilon}}}^{*J} = \underset{\approx}{\mathbf{B}}_*^{I} : \underset{\sim}{\boldsymbol{\Sigma}} + \sum_J \underset{\approx}{\mathbf{F}}_*^{IJ} : \widehat{\underset{\sim}{\boldsymbol{\varepsilon}}}^{*J}$ and $\widehat{\underset{\sim}{\boldsymbol{\varepsilon}}}^{*J} = \sum_{\beta(J)} f_{\beta(J)} \underset{\approx}{\mathbf{B}}_*^{t\beta(J)} : \underset{\sim}{\boldsymbol{\varepsilon}}^{*\beta(J)}$ respectively the effective stress and the effective eigen-strain in the heterogeneous domains I and J. In Eq. (2) we have introduced the notations:

$$\underset{\approx}{\mathbf{B}}_*^{\alpha_I} = \underset{\approx}{\mathbf{B}}_*^{\alpha(I)} : \underset{\approx}{\mathbf{B}}_*^{I}; \quad \underline{\underset{\approx}{\mathbf{F}}}_*^{\alpha_I\beta_J} = \frac{1}{f_{\beta_J}} \underset{\approx}{\mathbf{F}}_*^{\alpha_I\beta_J} = \underset{\approx}{\mathbf{B}}_*^{\alpha(I)} : \underline{\underset{\approx}{\mathbf{F}}}_*^{IJ} : \underset{\approx}{\mathbf{B}}_*^{t\beta(J)} + \frac{\delta^{IJ}}{f_J} \underline{\underset{\approx}{\mathbf{F}}}_*^{\alpha(I)\beta(I)}; \quad f_{\beta_J} = f_J f_{\beta(J)}, \tag{3}$$

that allow to simplify double summations $\sum_I \sum_{\alpha(I)} \underset{\approx}{\mathbf{X}}^{\alpha(I)}$ into single ones $\sum_{\alpha_I} \underset{\approx}{\mathbf{X}}^{\alpha_I}$. The asterisks indicate that the affine approximation refers, in each homogeneous nonlinear sub-domain $\alpha(I)$, to a linear comparison material of moduli $\underset{\approx}{\mathbf{C}}_*^{\alpha(I)}$. With $\underset{\sim}{\boldsymbol{\varepsilon}}^{\alpha(I)}$ denoting the mean total strain over sub-domain $\alpha(I)$, and with $\underset{\sim}{\boldsymbol{\sigma}}^{\alpha(I)}(\underset{\sim}{\boldsymbol{\varepsilon}}^{\alpha(I)}) = \underset{\sim}{\boldsymbol{\sigma}}^{\alpha(I)}$ the corresponding mean stress, the linearization procedure results from the first order Taylor's expansion:

$$\underset{\sim}{\boldsymbol{\sigma}}^{\alpha(I)}(\underset{\sim}{\boldsymbol{\varepsilon}}^{\alpha(I)}) = \underset{\sim}{\boldsymbol{\sigma}}_0^{\alpha(I)} + (\underset{\sim}{\boldsymbol{\varepsilon}}^{\alpha(I)} - \underset{\sim}{\boldsymbol{\varepsilon}}_0^{\alpha(I)}) : \left. \frac{\partial \underset{\sim}{\boldsymbol{\sigma}}^{\alpha(I)}}{\partial \underset{\sim}{\boldsymbol{\varepsilon}}^{\alpha(I)}} \right|_{\underset{\sim}{\boldsymbol{\varepsilon}}_0^{\alpha(I)}} = \underset{\approx}{\mathbf{C}}_*^{\alpha(I)} : (\underset{\sim}{\boldsymbol{\varepsilon}}^{\alpha(I)} - \underset{\sim}{\boldsymbol{\varepsilon}}^{*\alpha(I)}),$$

where $\underset{\sim}{\boldsymbol{\sigma}}_0^{\alpha(\mathrm{I})} = \underset{\sim}{\boldsymbol{\sigma}}^{\alpha(\mathrm{I})}(\underset{\sim}{\boldsymbol{\varepsilon}}_0^{\alpha(I)})$, $\underset{\approx}{\mathbf{C}}_*^{\alpha(I)} = \left. \frac{\partial \underset{\sim}{\boldsymbol{\sigma}}^{\alpha(\mathrm{I})}}{\partial \underset{\sim}{\boldsymbol{\varepsilon}}^{\alpha(\mathrm{I})}} \right|_{\underset{\sim}{\boldsymbol{\varepsilon}}_0^{\alpha(\mathrm{I})}} = (\underset{\approx}{\mathbf{S}}_*^{\alpha(I)})^{-1}$ and $\underset{\sim}{\boldsymbol{\varepsilon}}^{*\alpha(\mathrm{I})} = \underset{\sim}{\boldsymbol{\varepsilon}}_0^{\alpha(I)} - \underset{\approx}{\mathbf{S}}_*^{\alpha(I)} : \underset{\sim}{\boldsymbol{\sigma}}_0^{\alpha(I)}$.

The stress concentration tensors $(\underset{\approx}{\mathbf{B}}_*^{\alpha(I)}, \underset{\approx}{\mathbf{B}}_*^{I})$ and the stress influence tensors $(\underline{\underset{\approx}{\mathbf{F}}}_*^{\alpha(I)\beta(I)}, \underline{\underset{\approx}{\mathbf{F}}}_*^{IJ})$ in Eqs. (2) and (3) depend on the current effective tangent elastic–plastic moduli of the material $\underset{\approx}{\mathbf{C}}_*^{\mathrm{eff}} = (\sum_I \sum_{\alpha(I)} \underset{\approx}{\mathbf{S}}_*^{\alpha(I)} : \underset{\approx}{\mathbf{B}}_*^{\alpha(I)})^{-1}$ according to the implicit self-consistent scheme (Hill, 1965). Let us then denote $\tau^{g(\alpha(I))} = \tau^{g(\alpha_I)} = \mathbf{n}^{s(\alpha_I)} \underset{\sim}{\boldsymbol{\sigma}}^{\alpha_I} \mathbf{m}^{g(\alpha_I)} = \underset{\sim}{\mathbf{R}}^{g(\alpha_I)} : \underset{\sim}{\boldsymbol{\sigma}}^{\alpha_I} \geqslant 0$ the current applied resolved shear stress (ARSS) on a slip system g in a domain $\alpha(I)$. It is positive by definition of slip directions and, as given by Eq. (2), it takes the form:

$$\tau^{g(\alpha_I)} = \underset{\sim}{\mathbf{R}}^{g(\alpha_I)} : \underset{\approx}{\mathbf{B}}_*^{\alpha_I} : \underset{\sim}{\boldsymbol{\Sigma}} + \sum_{\beta_J} \underset{\sim}{\mathbf{R}}^{g(\alpha_I)} : \underset{\approx}{\mathbf{F}}_*^{\alpha_I\beta_J} : \underset{\sim}{\boldsymbol{\varepsilon}}^{*\beta_J} = \underset{\sim}{\mathbf{M}}_*^{g(\alpha_I)} : \underset{\sim}{\boldsymbol{\Sigma}} + \sum_{\beta_J} f_{\beta_J} \underset{\sim}{\mathbf{R}}^{g(\alpha_I)} : \underline{\underset{\approx}{\mathbf{F}}}_*^{\alpha_I\beta_J} : \underset{\sim}{\boldsymbol{\varepsilon}}^{*\beta_J}. \tag{4}$$

The tensors $\mathbf{M}_*^{g(\alpha_I)}$ are (i,j) symmetric due to the symmetry of $\underset{\sim}{\boldsymbol{\Sigma}}$. According to Eq. (1), the consistency condition for the plastic flow reads:

$$\mathrm{d}F0 = (F0, \underset{\sim}{\boldsymbol{\Sigma}})\mathrm{d}\underset{\sim}{\boldsymbol{\Sigma}} + \sum_{\beta_J}\sum_{k(\beta_J)}(F0, \bar{\gamma}^{k(\beta_J)})\mathrm{d}\bar{\gamma}^{k(\beta_J)} = 0, \tag{5}$$

with $\mathrm{d}\bar{\gamma}^{k(J)} = f_J\,\mathrm{d}\gamma^{k(J)}$ being the average slip increments over V and with

$$\begin{aligned} F0, \underset{\sim}{\boldsymbol{\Sigma}} &= \sum_{\alpha_I}\sum_{g(\alpha_I)} f_{\alpha_I}\left(\frac{\tau^{g(\alpha_I)}}{\tau_c^{g(\alpha_I)}}\right)^{n-1}\frac{\underset{\sim}{\mathbf{M}}_*^{g(\alpha_I)}}{\tau_c^{g(\alpha_I)}} \\ &= \sum_{\alpha_I}\sum_{g(\alpha_I)} f_{\alpha_I} P0^{g(\alpha_I)}\underset{\sim}{\mathbf{M}}_*^{g(\alpha_I)} = \sum_{\alpha_I}\sum_{g(\alpha_I)}\overline{P}0^{g(\alpha_I)}\underset{\sim}{\mathbf{M}}_*^{g(\alpha_I)} = \underset{\sim}{\mathbf{N}}\,0_*, \end{aligned} \tag{6a}$$

$$F0, \bar{\gamma}^{k(\beta_J)} = \sum_{\alpha_I}\sum_{g(\alpha_I)} f_{\alpha_I}\left(\frac{\tau^{g(\alpha_I)}}{\tau_c^{g(\alpha_I)}}\right)^{n-1}\left(\frac{\tau^{g(\alpha_I)}}{\tau_c^{g(\alpha_I)}}, \bar{\gamma}^{k(\beta_J)}\right) = -\sum_{\alpha_I}\sum_{g(\alpha_I)}\overline{P}0^{g(\alpha_I)}\underset{\sim}{\widetilde{H}}_{\Sigma}^{g(\alpha_I)k(\beta_J)}. \tag{6b}$$

In Eq. (6b), the modulus $\underset{\sim}{\widetilde{H}}_{\Sigma}^{g(\alpha_I)k(\beta_J)}$ takes the form:

$$\underset{\sim}{\widetilde{H}}_{\Sigma}^{g(\alpha_I)k(\beta_J)} = \left(\underset{\sim}{h}^{g(\alpha_I)k(\beta_J)}\left(\frac{\tau^{g(\alpha_I)}}{\tau_c^{g(\alpha_I)}}\right) - \underset{\sim}{\phi}_*^{g(\alpha_I)k(\beta_J)}\right) - (\underset{\sim}{\mathbf{R}}^{g(\alpha_I)} : \underset{\approx}{\mathbf{F}}_*^{\alpha_I\beta_J} : \underset{\sim}{\mathbf{R}}_*^{k(\beta_J)} + \underset{\sim}{\Phi}_*^{g(\alpha_I)k(\beta_J)}), \tag{7}$$

with

$$\underset{\sim}{h}^{g(\alpha_I)k(\beta_J)} = \tau_c^{g(\alpha_I)}, \bar{\gamma}^{k(\beta_J)}; \underset{\sim}{\phi}_*^{g(\alpha_I)k(\beta_J)} = (\underset{\sim}{\mathbf{R}}^{g(\alpha_I)}, \bar{\gamma}^{k(\beta_J)}) : \underset{\sim}{\boldsymbol{\sigma}}^{\alpha_I}, \tag{8a}$$

$$\underset{\sim}{\mathbf{R}}_*^{k(\beta_J)} = \underset{\sim}{\boldsymbol{\varepsilon}}^{*\beta_J}, \bar{\gamma}^{k(\beta_J)} \tag{8b}$$

and

$$\underset{\sim}{\Phi}_*^{g(\alpha_I)k(\beta_J)} = \underset{\sim}{\mathbf{R}}^{g(\alpha_I)} : ((\underset{\approx}{\mathbf{B}}_*^{\alpha_I}, \bar{\gamma}^{k(\beta_J)}) : \underset{\sim}{\boldsymbol{\Sigma}} + \sum_{\eta_L} f_{\eta_L}(\underset{\approx}{\mathbf{F}}_*^{\alpha_I\eta_L}, \bar{\gamma}^{k(\beta_J)}) : \underset{\sim}{\boldsymbol{\varepsilon}}^{*\eta_L}). \tag{8c}$$

The evolution of the critical resolved shear stress (CRSS) $\tau_c^{g(\alpha_I)}$ on each slip system g of each sub-domain $\alpha(I)$ results from a physical hardening law based on dislocation multiplications and interactions (Franciosi, 1988; Kocks et al., 1991). We here take it directly at the slip system scale of the form:

$$\mathrm{d}\tau_c^{g(\alpha_I)} = \sum_{\beta_J}\sum_{k(\beta_J)}^{N^{(t)}} h^{g(\alpha_I)k(\beta_J)}\mathrm{d}\gamma^{k(\beta_J)} = \sum_{\beta_J}\sum_{k(\beta_J)}^{N^{(t)}}\underset{\sim}{h}^{g(\alpha_I)k(\beta_J)}\mathrm{d}\bar{\gamma}^{k(\beta_J)}, \tag{9}$$

such that $\tau_c^{g(\alpha_I)} \geqslant \tau_0 > 0$ at any instant of the load, while slip systems of different kinds t possibly have different initial thresholds $\tau_0^{(t)}$. When considering a local hardening law rather than a non-local one (Berveiller et al., 1993), the only non-zero terms in the hardening matrix $[h]$ are for $\alpha(I) = \beta(J)$. For a totally homogeneous medium, one has $\underset{\approx}{\mathbf{B}}_*^{\alpha_I} = \underset{\approx}{\mathbf{I}}\ \forall\alpha_I$ and $\underset{\approx}{\mathbf{F}}_*^{\alpha_I\beta_J} = \underset{\approx}{\mathbf{0}}\ \forall\alpha_I, \beta_J$, what corresponds to no summation over domains $\alpha(I)$, such that $\underset{\sim}{\widetilde{H}}_{\Sigma}^{g(\alpha_I)k(\beta_J)} = \underset{\sim}{\widetilde{H}}_{\Sigma}^{gk}$. In the simplest case where the parameters are updated after each iteration, $\underset{\sim}{\phi}_*^{g(\alpha_I)k(\beta_J)}$ and $\underset{\sim}{\Phi}_*^{g(\alpha_I)k(\beta_J)}$ can be neglected in Eq. (7) which simplifies into:

$$\underset{\sim}{\widetilde{H}}_{\Sigma}^{g(\alpha_I)k(\beta_J)} = \left(\underset{\sim}{h}^{g(\alpha_I)k(\beta_J)}\left(\frac{\tau^{g(\alpha_I)}}{\tau_c^{g(\alpha_I)}}\right)\right) - \left(\underset{\sim}{\mathbf{R}}^{g(\alpha_I)} : \underset{\approx}{\mathbf{F}}_*^{\alpha_I\beta_J} : \underset{\sim}{\mathbf{R}}_*^{k(\beta_J)}\right). \tag{10}$$

However, this formulation of the affine type remains of complex use for aggregates since in addition to the iterative self-consistent procedure that provides the effective moduli, a second iteration is needed in each calculation step to obtain the current linear comparison moduli $\underset{\approx}{\mathbf{C}}_{*}^{\alpha(I)}$ of each phase $\alpha(I)=\alpha_I$. In comparison, a possible current partition of the material into plastically homogeneous domains would allow the simplifying use of the transformation field analysis (TFA) framework (Dvorak and Bahei-El-Din, 1997; Suquet, 1997). Slightly anticipating the next sections, it is worth to precise from now what we here mean by "partition". Suquet (1997) stressed that in general the TFA would only be exact in the limit where each point of the medium is considered a sub-domain. Therefore, in practice, such a spatial partition, which furthermore is step-wise evolving, is not achievable in a fully deterministic way. As a relevant alternative, Michel and Suquet (2003, 2004) considered partitions defined as some superimpositions of identified elementary heterogeneous (non-uniform) solutions. They established that when conveniently coupling such elementary "modes", accurate overall estimates were obtained. However, both the classic TFA and the non-uniform (NTFA) frameworks can be similarly associated to the RSL, as now summarized prior to specializing.

2.2. The transformation field analysis (TFA) framework in the RSL for poly-crystals

If the plastic field can be currently specified in the material, we can use the TFA method of homogenization that amounts to considering the local Hooke's elastic law as the current linear comparison material at $\mathbf{r}$. Then, in plastically homogeneous domains $\alpha(I)=\alpha_I$ of uniform elasticity moduli $\underset{\approx}{\mathbf{C}}^{\alpha_I}$ and with uniform plastic strain $\underset{\sim}{\boldsymbol{\varepsilon}}^{P\alpha_I}$, the mean stress $\underset{\sim}{\boldsymbol{\sigma}}^{\alpha_I}$ over $V_{\alpha_I}=f_{\alpha_I}V$ reads:

$$\underset{\sim}{\boldsymbol{\sigma}}^{\alpha_I}=\underset{\approx}{\mathbf{C}}^{\alpha_I}:(\underset{\sim}{\boldsymbol{\varepsilon}}^{\alpha_I}-\underset{\sim}{\boldsymbol{\varepsilon}}^{P\alpha_I})=\underset{\approx}{\mathbf{B}}^{\alpha_I}:\underset{\sim}{\boldsymbol{\Sigma}}+\sum_{\beta_J}f_{\beta_J}\underset{\approx}{\mathbf{F}}^{\alpha_I\beta_J}:\underset{\sim}{\boldsymbol{\varepsilon}}^{P\beta_J}. \tag{11}$$

In this TFA framework, the plastic strains $\underset{\sim}{\boldsymbol{\varepsilon}}^{P\beta_J}$ of the domains $\beta(J)=\beta_J$ are the uniform eigen-strains $\underset{\sim}{\boldsymbol{\varepsilon}}^{*\beta_J}$ of Eq. (2), the stress concentration and influence tensors without asterisk in Eq. (11) correspond to $\underset{\approx}{\mathbf{C}}_{*}^{\alpha_I}=\underset{\approx}{\mathbf{C}}^{\alpha_I}$ and Eq. (8b) becomes $\underset{*}{\mathbf{R}}^{k(\beta_J)}=\underset{\sim}{\boldsymbol{\varepsilon}}^{P\beta_J}$, $\bar{\gamma}^{k(\beta_J)}=\mathbf{R}^{k(\beta_J)}$. Eq. (3) still holds (without asterisks) when at the two different levels, the influence operators do not correspond to same phase arrangements or morphologies. According to these two levels, the two contributions of the stress influence operators $\underset{\approx}{\mathbf{F}}^{\alpha_I\beta_J}$ from Eq. (3) read:

$$\underset{\approx}{\mathbf{F}}^{IJ}=\underset{\approx}{\mathbf{H}}^{I}\delta^{IJ}-f_J\underset{\approx}{\mathbf{L}}^{IJ}, \tag{12a}$$

$$\underset{\approx}{\mathbf{F}}^{\alpha(I)\beta(I)}=\underset{\approx}{\mathbf{H}}^{\alpha(I)}\delta^{\alpha(I)\beta(I)}-f_{\beta(I)}\underset{\approx}{\mathbf{L}}^{\alpha(I)\beta(I)}. \tag{12b}$$

The operators $\mathbf{H}^I$ and $\mathbf{L}^{IJ}$ in Eq. (12a) are obtained from the strain modified Green operator integral of congruent ellipsoidal grains denoted $\underset{\approx}{\mathbf{t}}^{I}=\underset{\approx}{\mathbf{t}}^{i}$ and from its dual stress counterpart $\underset{\approx}{\mathbf{t}}'^{i}=\underset{\approx}{\mathbf{C}}^{\mathrm{eff}}-\underset{\approx}{\mathbf{C}}^{\mathrm{eff}}:\underset{\approx}{\mathbf{t}}^{i}:\underset{\approx}{\mathbf{C}}^{\mathrm{eff}}$ as

$$\underset{\approx}{\mathbf{H}}^{I}=\underset{\approx}{\mathbf{H}}^{II}=-\underset{\approx}{\mathbf{t}}'^{i}:\underset{\approx}{\mathbf{B}}^{II}=-\underset{\approx}{\mathbf{B}}^{I}:\underset{\approx}{\mathbf{t}}'^{i}=-\underset{\approx}{\mathbf{t}}'^{i}:\underset{\approx}{\mathbf{Y}}^{I}:\underset{\approx}{\mathbf{t}}'^{i}<0, \tag{13a}$$

$$\underset{\approx}{\mathbf{L}}^{IJ}=\underset{\approx}{\mathbf{H}}^{I}:\underset{\approx}{\mathbf{B}}^{tJ}=\underset{\approx}{\mathbf{B}}^{I}:\underset{\approx}{\mathbf{H}}^{J}=\underset{\approx}{\mathbf{B}}^{I}:\underset{\approx}{\mathbf{t}}'^{i}:\underset{\approx}{\mathbf{B}}^{tJ}, \tag{13b}$$

with $\underset{\approx}{\mathbf{Y}}^{I}=\underset{\approx}{\mathbf{Y}}^{tI}=(\underset{\approx}{\mathbf{t}}'^{i}-\underset{\approx}{\mathbf{t}}'^{i}:\Delta\underset{\approx}{\mathbf{S}}^{I}:\underset{\approx}{\mathbf{t}}'^{i})^{-1}>0$, $\Delta\underset{\approx}{\mathbf{S}}^{I}=\underset{\approx}{\mathbf{S}}^{\mathrm{eff}}-\underset{\approx}{\mathbf{S}}^{I}$. It thus comes:

$$\underset{\approx}{\mathbf{F}}_{i}^{IJ}=f_J\underset{\approx}{\underline{\mathbf{F}}}_{i}^{IJ}=-\underset{\approx}{\mathbf{B}}^{I}:\underset{\approx}{\mathbf{t}}'^{i}\delta^{IJ}+f_J\underset{\approx}{\mathbf{B}}^{I}:\underset{\approx}{\mathbf{t}}'^{i}:\underset{\approx}{\mathbf{B}}^{tJ}=-\underset{\approx}{\mathbf{t}}'^{i}:\underset{\approx}{\mathbf{B}}^{tI}\delta^{IJ}+f_J\underset{\approx}{\mathbf{B}}^{I}:\underset{\approx}{\mathbf{t}}'^{i}:\underset{\approx}{\mathbf{B}}^{tJ}. \tag{14a}$$

For homogeneous elasticity ($\Delta \underset{\approx}{\mathbf{S}}^I = 0,\ \underset{\approx}{\mathbf{B}}^I = \underset{\approx}{\mathbf{I}}\ \forall I$), $\underset{\approx}{\mathbf{L}}^{IJ} = \underset{\approx}{\mathbf{H}}^I = \underset{\approx}{\mathbf{H}}^J = -\underset{\approx}{\mathbf{t}}'^{iI}$ and:

$$\underset{\approx}{\mathbf{F}}_i^{IJ} = f_J \underline{\underline{\mathbf{F}}}_i^{IJ} = (f_J - \delta^{IJ})\underset{\approx}{\mathbf{t}}'^{iI}. \tag{14b}$$

Similar relations hold for $\underset{\approx}{\mathbf{F}}^{\alpha(I)\beta(I)}$ in Eq. (12b), if it is a heterogeneity level where all the sub-domains are congruent and ellipsoidal, what includes laminate layers as equivalent to infinitely flat (oblate) spheroids. Similar relations otherwise hold at any heterogeneity sub-level with congruent ellipsoidal sub-domains, including laminate structures.

The incremental macroscopic stress $\mathrm{d}\underset{\sim}{\mathbf{\Sigma}}$ versus strain $\mathrm{d}\underset{\sim}{\mathbf{E}}$ relation reads:

$$\begin{aligned}\mathrm{d}\underset{\sim}{\mathbf{\Sigma}} &= \underset{\approx}{\mathbf{C}}^{\mathrm{eff}} : \left(\mathrm{d}\underset{\sim}{\mathbf{E}} - \sum_{\beta_J} \sum_{k(\beta_J)=1}^{N^{(t)}} (f_{\beta_J} \underset{\approx}{\mathbf{B}}^{t\beta_J} : \underset{\sim}{\mathbf{R}}^{k(\beta_J)} \mathrm{d}\bar{\gamma}^{k(\beta_J)})\right) \\ &= \underset{\approx}{\mathbf{C}}^{\mathrm{eff}} : \left(\mathrm{d}\underset{\sim}{\mathbf{E}} - \sum_{\beta_J} \sum_{k(\beta_J)=1}^{N^{(t)}} \underset{\sim}{\mathbf{M}}^{k(\beta_J)} \mathrm{d}\bar{\gamma}^{k(\beta_J)}\right),\end{aligned} \tag{15}$$

where $\mathrm{d}\underset{\sim}{\mathbf{E}}^P = \sum_{\beta_J} \sum_{k(\beta_J)=1}^{N^{(t)}} \underset{\sim}{\mathbf{M}}^{k(\beta_J)} \mathrm{d}\bar{\gamma}^{k(\beta_J)} = (F0, \underset{\sim}{\mathbf{\Sigma}})\mathrm{d}\lambda 0 = \underset{\sim}{\mathbf{N}}\, 0\, \mathrm{d}\lambda 0$, and:

$$\mathrm{d}\bar{\gamma}^{k(\beta_J)} = (F0, \tau^{k(\beta_J)})\mathrm{d}\lambda 0 = f_J P0^{k(\beta_J)} \mathrm{d}\lambda 0 = \overline{P}0^{k(\beta_J)} \mathrm{d}\lambda 0. \tag{16}$$

Solving Eq. (5) for a fully applied incremental stress tensor $\mathrm{d}\underset{\sim}{\mathbf{\Sigma}}$, the tangent plastic compliance tensor $\underset{\approx}{\mathbf{L}}^P$ in $\mathrm{d}\underset{\sim}{\mathbf{E}}^P = \underset{\approx}{\mathbf{L}}^P : \mathrm{d}\underset{\sim}{\mathbf{\Sigma}}$ takes the form:

$$\underset{\approx}{\mathbf{L}}^P = \frac{\underset{\sim}{\mathbf{N}}\, 0 \otimes \underset{\sim}{\mathbf{N}}\, 0}{H0_\Sigma} = (H0_\Sigma)^{-1} \sum_{\alpha_I, \beta_J} \sum_{g(\alpha_I), k(\beta_J)} (\overline{P}0^{g(\alpha_I)} (\underset{\sim}{\mathbf{M}}^{g(\alpha_I)} \otimes \underset{\sim}{\mathbf{M}}^{k(\beta_J)}) \overline{P}0^{k(\beta_J)}), \tag{17a}$$

with, from Eqs. (6), (7) and (10):

$$H0_\Sigma = \sum_{\alpha_I, \beta_J} \sum_{g(\alpha_I), k(\beta_J)} \overline{P}0^{g(\alpha_I)} \underline{\widetilde{H}}_\Sigma^{g(\alpha_I)k(\beta_J)} \overline{P}0^{k(\beta_J)}. \tag{17b}$$

The dual case of a fully prescribed incremental strain tensor $\mathrm{d}\,\mathbf{E}$ leads to the corresponding matrix $[\underline{\widetilde{H}}_E] = [\underline{\widetilde{H}}_\Sigma + \underset{\sim}{\mathbf{M}} : \underset{\approx}{\mathbf{C}}^{\mathrm{eff}} : \underset{\sim}{\mathbf{M}}]$. As for $[\underline{\widetilde{H}}_E]$, all "intermediate matrices" corresponding to intermediate complementary mixed loading conditions ($\mathrm{d}\Sigma_{\alpha\beta}, \mathrm{d}E_{\alpha'\beta'}$) where P stress increments and $6 - P$ strain increments are prescribed[1] are the sum of an applied strain component with $[\underline{\widetilde{H}}_\Sigma]$. Due to the $[\underset{\sim}{\mathbf{R}} : \underline{\underline{\mathbf{F}}} : \underset{\sim}{\mathbf{R}}]$ contribution in the matrix $[\underline{\widetilde{H}}_\Sigma]$, this matrix $[\underline{\widetilde{H}}_\Sigma]$ is always non-local and so are the matrix $[\underline{\widetilde{H}}_E]$ and all intermediate matrices. The two-terms decomposition of the moduli $\underline{\widetilde{H}}_\Sigma^{g(\alpha_I)k(\beta_J)}$ from Eqs. (7) and (10) results in a related decomposition of the modulus $H0_\Sigma$ in Eq. (17b) as $H0_\Sigma = H0^{(h,\phi)} + H0^{(\mathrm{RFR},\Phi)}$ where $H0^{(\mathrm{RFR},\Phi)} = H0^{\mathrm{TFA}} \approx H0^{(\mathrm{RFR})}$ and:

$$\begin{aligned}H0^{(\mathrm{RFR})} &= -\sum_{\alpha_I, \beta_J} \sum_{g(\alpha_I), k(\beta_J)} \overline{P}0^{g(\alpha_I)} (\underset{\sim}{\mathbf{R}}^{g(\alpha_I)} : \underline{\underline{\mathbf{F}}}^{\alpha_I \beta_J} : \underset{\sim}{\mathbf{R}}^{k(\beta_J)}) \overline{P}0^{k(\beta_J)} \\ &= -\sum_{\alpha_I, \beta_J} \sum_{g(\alpha_I), k(\beta_J)} (\overline{P}0^{g(\alpha_I)} (\underset{\sim}{\mathbf{R}}^{g(\alpha_I)} \otimes \underset{\sim}{\mathbf{R}}^{k(\beta_J)}) \overline{P}0^{k(\beta_J)}) :: \underline{\underline{\mathbf{F}}}^{\alpha_I \beta_J}.\end{aligned} \tag{18}$$

[1] Three additional conditions on the total rotation are also to be specified, as recalled in Franciosi and Zaoui (1991).

The TFA-due over-stiffness that results from $H0^{\mathrm{TFA}}$ in $H0_{\Sigma}$, for $[\underset{\approx}{\mathbf{F}}] \neq \underset{\approx}{0}$ is mostly given by $H0^{(\mathrm{RFR})}$ in Eq. (18). Due to $[\underset{\approx}{\mathbf{F}}]$ operators of the range of the elasticity moduli tensors $\underset{\approx}{\mathbf{C}}^{\alpha_I}$ of the phases $\alpha(I)$, one has for usual materials $[\widetilde{\underline{H}}_{\Sigma}] \approx [h - \underset{\sim}{\mathbf{R}} : \underset{\approx}{\mathbf{F}} : \underset{\sim}{\mathbf{R}}] \gg [h]$. But more precisely, the relative contributions to $[\widetilde{\underline{H}}_{\Sigma}]$ of the physical hardening $[h]$ and of the accommodation hardening $[-\underset{\sim}{\mathbf{R}} : \underset{\approx}{\mathbf{F}} : \underset{\sim}{\mathbf{R}}]$ will depend on features of the material morphology, namely the sub-domain definitions, shapes and arrangements, that may affect both terms, as it will be discussed in Section 4.

2.3. The case of twinning mechanisms with homogeneous intra-crystalline slip

For the two-level heterogeneity description considered from Eq. (3), the TFA-due part $H0^{(\mathrm{RFR})}$ of the effective stiffness reads, with Eqs. (11) and (12):

$$H0^{(\mathrm{RFR})} = -\sum_{I,J}\sum_{\alpha(I),\beta(J)}\left(\sum_{g(\alpha(I)),k(\beta(J))}(\overline{P}0^{g(\alpha(I))}\underset{\sim}{\mathbf{R}}^{g(\alpha(I))} \otimes \underset{\sim}{\mathbf{R}}^{k(\beta(J))}\overline{P}0^{k(\beta(J))})\right) :: \left(\underset{\approx}{\mathbf{F}}^{IJ} + \frac{\delta^{IJ}}{f_J}\underset{\approx}{\mathbf{F}}^{\alpha(I)\beta(J)}\right). \tag{19}$$

It shares into a contribution from the inter granular influence operators $\underset{\approx}{\mathbf{F}}^{IJ}$ and a contribution from the intra-crystalline ones $\underset{\approx}{\mathbf{F}}^{\alpha(I)\beta(J)}$ (with $\overline{P}0^{g(\alpha(I))} = f_I f_{\alpha(I)} P0^{g(\alpha(I))} = f_{\alpha_I} P0^{g(\alpha_I)}$). While the former operators $\underset{\approx}{\mathbf{F}}^{IJ}$ usually derive from the characteristic of the mean grain shape, taking the form given in Eqs. (14) for congruent ellipsoids with the particular simple expression of Eq. (14b) for homogeneous elasticity (alternative forms will be discussed in Section 4), the latter operators $\underset{\approx}{\mathbf{F}}^{\alpha(I)\beta(J)}$ are issued from the description given to the intra-crystalline plasticity. They vanish when the crystals are treated as plastically homogeneous, as it is allowed in first approximation when plastic strain results from slip. They do not vanish if twinning enters the process since twinned grains are no longer plastically homogeneous. With regard to twinning modes of plastic straining, it is noteworthy that almost all of the formalism of Sections 2.1 and 2.2 still holds. In particular, Eq. (9) can still be used to formally describe evolutions for the critical twinning shear stresses, although the appropriate inter-twinning or mixed slip-twin h^{gk} moduli are to be specified from microstructural arguments (Tranchant et al., 1993; Franciosi et al., 1993; Salem et al., 2005). If one considers that the $\alpha(I)$ partition of a grain I represents twinning, each domain $\alpha(I)$ corresponds to a single twinning system. The associated shear strain is still given by Eq. (16) that must be recast as

$$\mathrm{d}\bar{\gamma}^{T(\alpha_I)} = \gamma_0\,\mathrm{d}f_{\alpha_I} = (F0, \tau^{T(\alpha_I)})\,\mathrm{d}\lambda 0 = f_I P0^{T(\alpha_I)}\,\mathrm{d}\lambda 0 = \overline{P}0^{T(\alpha_I)}\,\mathrm{d}\lambda 0, \tag{20}$$

with $\gamma_0 > 0$ the elementary shear that results from the (geometrically specified) unit twin on the twinning system type. Eq. (20) is the positive evolution law for the volume fraction of the twinned crystal part $\alpha(I)$, the condition being that $\sum_{\alpha_I}(f_{\alpha_I} + \mathrm{d}f_{\alpha_I}) \leqslant 1$. During each increment, while the existing volume fraction f_{α_I} of twinned crystal can undergo slip, the twinning incremental activity $\mathrm{d}f_{\alpha_I}$ corresponds to a newly twinned part of lattice that is not allowed to slip.

As for the case of slip plasticity, the number of new twinned domains can increase at each calculation step, yielding to multiplicative branching that is difficult to track.

Formally, the effective plastic strain and stiffness for a twinned crystal can be obtained following the here proposed HML description of intra-crystalline slip. But since twinned crystal can hardly be reduced to an equivalent homogeneous single crystal of some mean orientation as it has been proposed for slip, a specific scenario should be considered. This will be commented later on. The next section recalls the characteristics of the intra-crystalline influence operators when slip (or twinning shear) is described in terms of multi-laminate structures.

3. A description of crystal plasticity into a hierarchical multi-laminate (HML) structure

Here, we briefly reconsider the HML structure that has been defined for slip only in Franciosi and Berbenni (2007) and we extend it to the case of twinning modes of crystal plasticity.

3.1. Definition of intra-crystalline HML structures for slip and no twinning

Assumption (a): the successive laminates are parallel to the different crystallographic orientations of the slip planes, disregarding the details of compatibility and equilibrium restrictions. As far as a single slip plane orientation, "A" say, is currently active in some domain, the plastic strain is considered as homogeneous in the domain.[2] Permutations between the P crystallographic slip planes A, B, C,... form a number $P!$ of hierarchical multi-laminate (HML) structures for slip, of rank $(P-1)$, that we denote $(P-1)-$HML. For (1 1 1) octahedral slip planes in FCC crystals for example, $P=4$ and $P!=4!=24$ is the number of possible (3)-HML structures for slip. In BCC crystals with $(1\,1\,0)\langle 1\,1\,1\rangle$systems, $P=6$ and the number of possible $(5)-$HML structures for slip is $P!=6!=720$, etc. Conversely, pure basal slip in HCP crystals would remain homogeneous;
Assumption (b): at any point $\mathbf{r}$ of the crystal, each possible $(P-1)-$HML structure $h=I|J|K|\cdots|(P)$ for slip, $h\in(1,P!)$, has the occurrence probability:

$$p^{(h)}=p^{(I|J|K|\cdots|(P))}=p(I)\left(\frac{p(J)}{1-p(I)}\right)\left(\frac{p(K)}{1-(p(I)+p(J))}\right)\cdots=\prod_{U=1}^{P-1}\left(\frac{p(U)}{1-\sum_{V=1}^{U-1}p(V)}\right), \tag{21a}$$

where $p(I)$ denotes the probability that the slip plane I defines the primary laminate orientation A. The connection of $p(I)$ to the relative incremental slip activity on the slip planes is taken of the form:

$$p(I)=\frac{\mathrm{d}\gamma^{I}}{\sum_{I}\mathrm{d}\gamma^{I}}=\frac{\sum_{g(I)}\mathrm{d}\gamma^{g(I)}}{\sum_{I}\sum_{g(I)}\mathrm{d}\gamma^{g(I)}}=\frac{\sum_{g(I)}P0^{g(I)}}{\sum_{I}\sum_{g(I)}P0^{g(I)}}. \tag{21b}$$

According to Eq. (21b), special cases of importance are the symmetric loading situations with several equally active planes, for which several HML structures will be equally probable. But in general, because $n\gg 1$ in the flow criterion of Eq. (1), even for small differences of applied resolved shear stresses between the slip systems of dif-

[2] The laminate nature of planar slip where elastic layers of material separate bands of concentrated slip is here disregarded, for sake of simplicity, but it could be entered in the description if of interest.

ferent slip planes, the different $(P-1)-$HML structures (h) for slip will be ordered in terms of their occurrence probability $p^{(h)}$ from one dominant "mode" to a majority of negligible ones, in proportion of their relative incremental slip activities. Compared occurrence probability distributions $p^{(h)}$ for $P=4$ slip planes π with a single slip system $g(\pi)$on each are reported for $n=2$ and $n=20$ in Fig. 1, for arbitrary relative applied resolved shear stresses $\tau^{g(\pi)}$ for the Primary (P), Secondary (S), Ternary (T) and Quaternary (Q) planes. The ARSSs $\tau^{g(\pi)}$ are taken in proportion with the values (9, 8, 7, 6) while a same CRSS value τ_0 is assumed for all the $P0^{g(\pi)}$coefficients introduced in Eqs. (6). These coefficients fix the slip increments from Eq. (16) and the occurrence probabilities of the $(P-1)-$HML structures for slip from Eq. (21b). The dominant $(3)-$HML structure for $n=20$ is clearly by far the $h=1|2|3|(4)=P|S|T|(Q)$ hierarchy for which $\mathrm{d}\gamma^1 \gg \mathrm{d}\gamma^2 > \mathrm{d}\gamma^3 > \mathrm{d}\gamma^4$;

Assumption (c): a statistically homogeneous $(P-1)-$HML structure for slip can be defined from the superposition of the $P!$ heterogeneous plastic modes (h), weighted by their occurrence probabilities $p^{(h)}$. This superposition also removes or at least smoothes out the length-scale hierarchy limitations between each lamination rank as well as the compatibility and equilibrium restrictions for the individual $(P-1)-$HML structures for slip which have been disregarded so far. Once this superposition of the $P!$ possible modes is achieved for the increment, the heterogeneous description of the crystal plasticity reduces to a P-partition of the crystal I, whose sub-domains $\alpha(I)$ support different plastic strains. This statistically defined P-partition finally corresponds to a morphology that is described by a $P\times P$ matrix of mean stress (resp. strain) influence operators. In each crystal I, these mean stress influence tensors take the form $\langle \underset{\approx}{\mathbf{F}}^{\alpha(I)\beta(I)}\rangle = \sum_{h=1}^{P!} p^{(h)} \underset{\approx}{\mathbf{F}}^{(h)\alpha(I)\beta(I)}$, where each $(P-1)-$HML solution (h) contributes for one operator $\underset{\approx}{\mathbf{F}}^{(h)\alpha(I)\beta(I)}$. Note that in practice, the triggering of heterogeneous intra-crystalline slip without a non-local behavior law

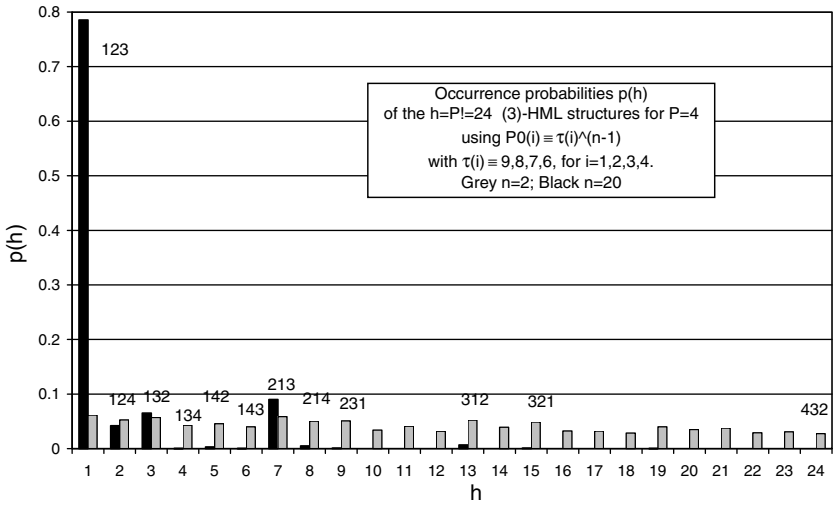

Fig. 1. Compared sets, for $n=2$ and $n=20$ in Eq. (1), of the $h=P!=24$ occurrence probability values $p(h)$ for the (3)-HML structures realizable with $P=4$ slip planes π. We consider one single slip system per plane $g(\pi)$, all of same CRSS τ_0, and we take ARSS values $\tau^{g(\pi)}$ proportional to $(9,8,7,6)$ such that from Eq. (16) $P0^{g(\pi)} \equiv (\tau^{g(\pi)})^{(n-1)}$.

needs some initial lattice disorientation (mosaic), or spatial fluctuation in the critical resolved shear stresses.

3.2. Relevancy of HML structures for twinning

Difficulties to mix slip and twinning mechanisms are avoided when dissociating incremental twinning events from slip ones as pointed in Section 2.3. We consequently need to consider the relevancy of HML structures for the description of twinning modes alone. Twinning planes (resp. directions) may or may not coincide with slip planes (resp. directions), but twinning systems never are slip systems as well and conversely.

The main differences between slip and twinning systems in the present context are:

- coplanar twinning systems need to be treated as individuals and they make possible one-layered structures of more than two phases;
- twinning systems are always not symmetric with regard to the twin direction, as is for example the case for $(1\,1\,1)\langle 1\,1\,2\rangle$ systems in FCC crystals;[3]
- disregarding lattice mismatches, the disorientation of twinned domains with regard to an initial grain is a fixed non-zero value while it is zero for slip. Starting from one crystal orientation, the set of twinned disorientations is finite but successive (hierarchical) twinning operations generally do not create a closed finite set of orientations;
- a single active twinning system is enough to create a heterogeneous crystalline structure, what is also true for a single active slip plane at small enough scale (slip bands separated by slip-free layers) but in contrast with slip this heterogeneity cannot be disregarded;

As a consequence, if the proposed HML incremental description for heterogeneous multi-planar slip is formally applicable to multiple twinning, step-wise averaging cannot be performed as for slip. At each step the number of crystalline orientations in the homogeneous equivalent super crystal is potentially multiplied by P, even if each new sub-level contributes decreasingly enough to allow a finite (truncated) branching. However, since a twinned crystal is definitely a multi-crystal, the case of twinning plastic modes can be more naturally reconsidered in the context of the extension of the RSL–TFA–HML modeling to poly-crystals of homogeneous domains, to be discussed later on.

3.3. Constitutive equations for intra-crystalline HML structures for slip or twinning

For short, regardless of the slip or twinning nature of the P plastic strain mechanisms that are to be accounted for, one can write for each possible $(P-1)-$HML structure (omitting the superscript "h") the stress increments of the P phases in terms of the plastic strain ones as

$$\mathrm{d}\underset{\sim}{\boldsymbol{\sigma}}^{\pi} = (\underset{\approx}{\mathbf{B}}^{\pi}) : \mathrm{d}\,\underset{\sim}{\boldsymbol{\Sigma}} + \sum_{\pi'} (\underset{\approx}{\mathbf{F}}^{\pi\pi'}) : \mathrm{d}\underset{\sim}{\boldsymbol{\varepsilon}}^{P\pi'} = (\underset{\approx}{\mathbf{B}}^{\pi}) : \mathrm{d}\,\underset{\sim}{\boldsymbol{\Sigma}} + \sum_{\pi'} f_{\pi'} (\underset{\approx}{\underline{\mathbf{F}}}^{\pi\pi'}) : \mathrm{d}\underset{\sim}{\boldsymbol{\varepsilon}}^{P\pi'}. \tag{22}$$

The involved operators $(\underset{\approx}{\mathbf{B}}^{\pi})$ and $(\underset{\approx}{\underline{\mathbf{F}}}^{\pi\pi'})$, for $\pi, \pi' \in (1, P)$, are special cases of the operators $(\underset{\approx}{\mathbf{B}}^{\alpha(I)})$ and $(\underset{\approx}{\underline{\mathbf{F}}}^{\alpha(I)\beta(I)})$ of Eq. (11) for a crystal-like sub-domain I. In order to establish key

[3] Slip systems may also be asymmetric, like $(1\,1\,2)\langle 1\,1\,1\rangle$ slip systems in BCC crystals for example.

characteristics, their general forms need to be explicated. For each of the $(P-1)-$HML structures among $P!$ ones, each one of the P stress concentration tensors ($\underset{\approx}{\mathbf{B}}^{\pi}$) in Eq. (22) is a product ($\underset{\approx}{\mathbf{B}}^{\pi}_{k/k-1} : \underset{\approx}{\mathbf{B}}^{\pi\eta}_{k-1/k-2} : \cdots : \underset{\approx}{\mathbf{B}}^{\pi\eta\ldots\phi}_{1/0}$) of k stress concentration tensors that links the level $k \in (1, P-1)$ where the phase π is located to the macroscopic level (0). Similarly, the $P \times P$ stress influence tensors ($\underset{\approx}{\underline{\mathbf{F}}}^{\pi\pi'}$) are linear combinations of $(P-1)$ elementary influence tensors $\underset{\approx}{\underline{\mathbf{F}}}^{\kappa\kappa'}_{l}$, one for each lamination level $l \in (1, P-1)$, that are characterized by the laminate operator as given in Eqs. (13) and (14). Each of these operators are also a sum of several contributions which have the general form that links the level l of a laminate to the level k of the phase π on the left "stress" side of Eq. (22) and to the level k' of the phase π' on the right "strain" side of Eq. (22) as

$$(\underset{\approx}{\mathbf{B}}^{\pi\eta\cdots\kappa}_{k/k-1} : \underset{\approx}{\mathbf{B}}^{\eta\cdots\kappa}_{k-1/k-2} : \cdots : \underset{\approx}{\mathbf{B}}^{\kappa}_{l+1/l}) : \underset{\approx}{\underline{\mathbf{F}}}^{\kappa\kappa'}_{l} : (\underset{\approx}{\mathbf{B}}^{t\kappa'}_{l/l+1} : \cdots : \underset{\approx}{\mathbf{B}}^{t\kappa'\cdots\eta'}_{k'-2/k'-1} : \underset{\approx}{\mathbf{B}}^{t\kappa'\cdots\eta'\pi'}_{k'-1/k'}) = (\underset{\approx}{\mathbf{B}}^{\pi}_{k}) : \underset{\approx}{\underline{\mathbf{F}}}^{\kappa\kappa'}_{l} : (\underset{\approx}{\mathbf{B}}^{\pi'}_{k'}).$$

The phase π referring to the slip on plane π, these products can be expressed more simply when laminate levels also correspond to slip planes π''. Furthermore, from Eqs. (13) and (14), the elementary influence operators $\underset{\approx}{\underline{\mathbf{F}}}^{\pi\pi'}_{\pi''}$ at each level are either of the form of a product $f_{\pi'}\underset{\approx}{\mathbf{B}}^{\pi}_{\pi''} : \underset{\approx}{\mathbf{t}}'^{\pi'\prime}_{C\pi''} : \underset{\approx}{\mathbf{B}}^{\pi'}_{\pi''}$, when $\pi \neq \pi'$, or of minus a sum $\sum_{\kappa\neq\pi'} f_{\kappa}\underset{\approx}{\mathbf{B}}^{\kappa}_{\pi''} : \underset{\approx}{\mathbf{t}}'^{\pi'\prime}_{C\pi''} : \underset{\approx}{\mathbf{B}}^{\pi'}_{\pi''}$ of such products when $\pi = \pi'$ (from using $\underset{\approx}{\mathbf{I}} = \sum_{\pi'} f_{\pi'}\underset{\approx}{\mathbf{B}}^{\pi'}$), where the laminate operator $\underset{\approx}{\mathbf{t}}'^{\pi'\prime}_{C\pi''}$ depends on the moduli tensor $\underset{\approx}{\mathbf{C}}^{\pi''}$. It is therefore enough for the present purpose to point that each operator ($\underset{\approx}{\underline{\mathbf{F}}}^{\pi\pi'}$) can be written as a sum:

$$(\underset{\approx}{\underline{\mathbf{F}}}^{\pi\pi'}) = \sum_{\pi''=1}^{P-1} \xi^{\pi\pi'}_{\pi''}(\underset{\approx}{\mathbf{B}}^{\pi}) : \underset{\approx}{\underline{\mathbf{F}}}^{\pi\pi'}_{\pi''} : (\underset{\approx}{\mathbf{B}}^{\pi'}) = \sum_{\pi''=1}^{P-1} \xi^{\pi\pi'}_{\pi''}(\underset{\approx}{\mathbf{B}}^{\pi}) : \left(\sum_{\kappa} \zeta_{\kappa}\underset{\approx}{\mathbf{B}}^{\kappa}_{\pi''} : \underset{\approx}{\mathbf{t}}'^{\pi''}_{C\pi''} : \underset{\approx}{\mathbf{B}}^{\pi'}_{\pi''}\right) : (\underset{\approx}{\mathbf{B}}^{\pi'}), \tag{23}$$

where each term takes the form $(\underset{\approx}{\mathbf{B}}^{\pi}_{\pi''}) : \underset{\approx}{\mathbf{t}}'^{\pi''}_{C\pi''} : (\underset{\approx}{\mathbf{B}}^{\pi'}_{\pi''})$, with $(\underset{\approx}{\mathbf{B}}^{\pi}_{\pi}) = (\underset{\approx}{\mathbf{B}}^{\pi'}_{\pi'}) = \underset{\approx}{\mathbf{I}}$.

From Eq. (22), neglecting the partial derivatives with respect to the plastic slip or twinning shear $\gamma^{k(\pi')}$ of the terms that correspond to the $[\phi]$ and $[\Phi]$ matrix terms in Eq. (7), the ARSSs on the $g(\pi)$ mechanism can be expressed as

$$\mathrm{d}\tau^{g(\pi)} = \underset{\sim}{\mathbf{R}}^{g(\pi)} : \mathrm{d}\underset{\sim}{\boldsymbol{\sigma}}^{\pi} = \underset{\sim}{\mathbf{R}}^{g(\pi)} : (\underset{\approx}{\mathbf{B}}^{\pi}) : \mathrm{d}\,\underset{\sim}{\boldsymbol{\Sigma}} + \sum_{\pi'}\sum_{k(\pi')} f_{\pi'}\underset{\sim}{\mathbf{R}}^{g(\pi)} : (\underset{\approx}{\underline{\mathbf{F}}}^{\pi\pi'}) : \underset{\sim}{\mathbf{R}}^{k(\pi')}\mathrm{d}\gamma^{k(\pi')}. \tag{24}$$

According to the form of ($\underset{\approx}{\underline{\mathbf{F}}}^{\pi\pi'}$) from Eq. (23), in each product $\underset{\sim}{\mathbf{R}}^{g(\pi)} : (\underset{\approx}{\mathbf{B}}^{\pi}_{\pi''}) : \underset{\approx}{\mathbf{t}}'^{\pi''}_{C\pi''} : (\underset{\approx}{\mathbf{B}}^{\pi'}_{\pi''}) : \underset{\sim}{\mathbf{R}}^{k(\pi')}$ the equalities $\underset{\sim}{\mathbf{R}}^{g(\pi)} : (\underset{\approx}{\mathbf{B}}^{\pi}_{\pi''}) = (\underset{\approx}{\mathbf{B}}^{t\pi}_{\pi''}) : \underset{\sim}{\mathbf{R}}^{g(\pi)} = (\underset{\sim}{\mathbf{M}}^{g(\pi)}_{\pi''})$ hold such that the individual terms of the operators $\underset{\sim}{\mathbf{R}}^{g(\pi)} : (\underset{\approx}{\underline{\mathbf{F}}}^{\pi\pi'}) : \underset{\sim}{\mathbf{R}}^{k(\pi')}$ can be also expressed as $(\underset{\sim}{\mathbf{M}}^{g(\pi)}_{\pi''}) : \underset{\approx}{\mathbf{t}}'^{\pi''}_{C\pi''} : (\underset{\sim}{\mathbf{M}}^{k(\pi')}_{\pi''})$.

Among the general properties of these stress influence tensors ($\underset{\approx}{\underline{\mathbf{F}}}^{\pi\pi'}$), coming first are the dependency conditions:

$$\begin{cases} \sum_{\pi'}(\underset{\approx}{\mathbf{F}}^{\pi\pi'}) = \sum_{\pi'} f_{\pi'}(\underset{\approx}{\underline{\mathbf{F}}}^{\pi\pi'}) = 0 \quad \forall\pi, \\ \sum_{\pi} f_{\pi}(\underset{\approx}{\mathbf{F}}^{\pi\pi'}) = \sum_{\pi} f_{\pi} f_{\pi'}(\underset{\approx}{\underline{\mathbf{F}}}^{\pi\pi'}) = 0 \quad \forall\pi', \end{cases} \tag{25}$$

respectively because equal plastic strain increments yield equal stress ones and because the mean stress increment equals $\mathrm{d}\underset{\sim}{\boldsymbol{\Sigma}}$. More specialized properties are recalled and examined further in the next sections.

3.4. Main characteristics of the $\underset{\approx}{\mathbf{F}}^{\pi\pi'}$ stress influence operators of HML structures

For homogeneous elasticity, what excludes twinning possibilities unless elasticity is isotropic, all stress concentration tensors reduce to the identity tensor and all the stress influence tensors $(\underset{\approx}{\mathbf{F}}^{\pi\pi'}) = f_{\pi'}(\underset{\approx}{\underline{\mathbf{F}}}^{\pi\pi'})$ of any $(P-1)-$HML structure among $P!$ are simple linear combinations of independent elementary operators $\underset{\approx}{\mathbf{t}}'^{\pi}_{C\pi}$, $\pi = A, B, C, \ldots$. Then, these influence operators for each different considered laminate hierarchy (h) can be written $(\underset{\approx}{\mathbf{F}}^{\pi\pi'})_{(h)} = f_{\pi'}(\underset{\approx}{\underline{\mathbf{F}}}^{\pi\pi'})_{(h)} = -\sum_{\pi''}\phi^{(h)\pi\pi'}_{\pi''}\underset{\approx}{\mathbf{t}}'^{\pi''}_{C\pi''}$, $\pi'' = A, B, C, \ldots, (P-1)$. The negative sign can be ignored in the discussion since it is compensated by the one present in Eq. (19). Similarly, any weighted superposition of the $P!$ different operators in terms of the occurrence probabilities of the corresponding $(P-1)-$HML structure remains a linear combination of the same elementary operators, to be denoted $\langle\underset{\approx}{\mathbf{F}}^{\pi\pi'}\rangle = -\sum_{\pi''}\langle\phi^{\pi\pi'}_{\pi''}\rangle\underset{\approx}{\mathbf{t}}'^{\pi''}_{C\pi''} = -\sum_{\pi''}\sum_{h=1}^{P!} p^{(h)}\phi^{(h)\pi\pi'}_{\pi''}\underset{\approx}{\mathbf{t}}'^{\pi''}_{C\pi''}$. In the case of a two-level homogenization scheme for each intra-crystalline contribution I, that also reads from Eq. (19), $f_{\pi'(I)}\langle\underset{\approx}{\underline{\mathbf{F}}}^{\pi(I)\pi'(I)}\rangle = -\sum_{\pi''I}\langle\phi^{\pi I\pi' I}_{\pi''I}\rangle\underset{\approx}{\mathbf{t}}'^{\pi''I}_{C\pi''I}$.

These operators $\underset{\approx}{\mathbf{t}}'^{\pi''}_{C\pi''}$ or $\underset{\approx}{\mathbf{t}}'^{\pi''I}_{C\pi''I}$ appearing in the terms $[\underset{\sim}{\mathbf{R}} : \underset{\approx}{\underline{\mathbf{F}}} : \underset{\sim}{\mathbf{R}}]$ of the part $H0^{(\mathrm{RFR})}$ part of the modulus $H0_{\Sigma}$, when considering a HML intra-crystalline structure, are the modified stress Green operator integrals for platelet domains (infinitely flat spheroids) respectively oriented as the A, B, C, ... laminate layers (of each grain or domain I). According to Eqs. (25), the weights $\phi^{(h)\pi\pi'}_{\pi''}$ of the decompositions of the operators $(\underset{\approx}{\mathbf{F}}^{\pi\pi'})_{(h)}$, for each laminate hierarchy (h), fulfill the relations:

$$\begin{cases} \sum_{\pi'}\phi^{(h)\pi\pi'}_{\pi''} = 0 \quad \forall\pi \ \ \forall\pi'', \\ \sum_{\pi}f_{\pi}\phi^{(h)\pi\pi'}_{\pi''} = 0 \quad \forall\pi' \ \ \forall\pi'' \end{cases} \tag{26}$$

and so does their average $\langle\phi^{\pi\pi'}_{\pi''}\rangle$.

For anisotropic heterogeneous elasticity, what is the general situation, especially when twinning occurs, because the HML structure corresponds to congruent domains (parallel layers) at each sub-level of heterogeneity, Eqs. (14) apply and the stress influence tensors issued from Eq. (24) can be expressed as a sum of terms $(\underset{\sim}{\mathbf{M}}^{g(\pi)}_{\pi''}) : \underset{\approx}{\mathbf{t}}'^{\pi''}_{C\pi''} : (\underset{\sim}{\mathbf{M}}^{k(\pi')}_{\pi''})$.

Then, when visiting the properties of these operators and the specific conditions for which the TFA accommodation contributions to the material stiffness may be reduced or may possibly cancel, it is noteworthy that the TFA excessive stiffness can generally be lowered down to realistic values for highly symmetric multiple plastic strain modes. This is due to the conditions of Eqs. (25) and (26) that yield to globally cancel terms $P0^{g(\pi)}\underset{\sim}{\mathbf{R}}^{g(\pi)} : (\underset{\approx}{\mathbf{F}}^{\pi\pi'}) : \underset{\sim}{\mathbf{R}}^{k(\pi')}P0^{k(\pi')}$ of the double sum in $H0^{\mathrm{TFA}}$ from Eqs. (18) and (19). Commonly to all morphology descriptions including laminate structures, this corresponds to triggering excessive multiple interactions and consequently excessive material hardening to reduce the accommodation stiffness. Here, enforced excessive (homogeneous) multiple

slip to reduce elastic accommodation appears to be the reason, not specifically to laminates, for the TFA over-stiffness.

The main specific property of the laminate structures that similarly results in a significant decrease of the TFA-due accommodation stiffness as pointed out in Franciosi and Berbenni (2007), is the so-called "orthogonality property", that is reconsidered in the next section from a more exhaustive viewpoint.

3.5. Orthogonality property of influence operators in HML structures

We here question how, specifically for laminate structures and not as a consequence of Eqs. (25), (26) only, can the products $(P0^{g(\pi)}\underset{\sim}{\mathbf{R}}^{g(\pi)} \otimes \underset{\sim}{\mathbf{R}}^{k(\pi')}P0^{k(\pi')}) :: (\underset{\approx}{\mathbf{F}}^{\pi\pi'})$ be individually or collectively cancelled for particular orientations of laminates with regard to those of slip systems. Individual situations which cancel some of the components $(\underset{\sim}{\mathbf{M}}^{g(\pi)}_{\pi''}) : \underset{\approx}{\mathbf{t}}'^{\pi''}_{C\pi''} : (\underset{\sim}{\mathbf{M}}^{k(\pi')}_{\pi''})$ correspond either to a null global product, involving a system pair $(g(\pi),k(\pi')) = (g,k)$, of the form:

$$(\underset{\sim}{\mathbf{M}}^{g(\pi)}_{\pi''}) : \underset{\approx}{\mathbf{t}}'^{\pi''}_{C\pi''} : (\underset{\sim}{\mathbf{M}}^{k(\pi')}_{\pi''}) = \underset{\approx}{\mathbf{t}}'^{\pi''}_{C\pi''} :: ((\underset{\sim}{\mathbf{M}}^{g(\pi)}_{\pi''}) \otimes (\underset{\sim}{\mathbf{M}}^{k(\pi')}_{\pi''})) = 0 \tag{27a}$$

or to null products with regard to a single involved system g or k, such as (see Eq. (26)):

$$(\underset{\sim}{\mathbf{M}}^{g(\pi)}_{\pi''}) : \underset{\approx}{\mathbf{t}}'^{\pi''}_{C\pi''} = 0 \quad \text{or} \quad \underset{\approx}{\mathbf{t}}'^{\pi''}_{C\pi''} : (\underset{\sim}{\mathbf{M}}^{k(\pi')}_{\pi''}) = 0. \tag{27b}$$

We exclude from the solutions of Eq. (27a) those which are the solutions of Eq. (27b).

Particular system groups can also collectively cancel double sums of terms $(\underset{\sim}{\mathbf{M}}^{g(\pi)}_{\pi''}) : \underset{\approx}{\mathbf{t}}'^{\pi''}_{C\pi''} : (\underset{\sim}{\mathbf{M}}^{k(\pi')}_{\pi''})$, or simple sums of terms $(\underset{\sim}{\mathbf{M}}^{g(\pi)}_{\pi''}) : \underset{\approx}{\mathbf{t}}'^{\pi''}_{C\pi''}$ or $\underset{\approx}{\mathbf{t}}'^{\pi''}_{C\pi''} : (\underset{\sim}{\mathbf{M}}^{k(\pi')}_{\pi''})$. For homogeneous elasticity (no twinning cases), Eqs. (27) respectively simplify into:

$$\underset{\sim}{\mathbf{R}}^{g(\pi)} : \underset{\approx}{\mathbf{t}}'^{\pi''}_{C\pi''} : \underset{\sim}{\mathbf{R}}^{k(\pi')} = \underset{\approx}{\mathbf{t}}'^{\pi''}_{C\pi''} :: (\underset{\sim}{\mathbf{R}}^{g(\pi)} \otimes \underset{\sim}{\mathbf{R}}^{k(\pi')}) = 0, \tag{28a}$$

$$\underset{\sim}{\mathbf{R}}^{g(\pi)} : \underset{\approx}{\mathbf{t}}'^{\pi''}_{C\pi''} = 0 \quad \text{or} \quad \underset{\approx}{\mathbf{t}}'^{\pi''}_{C\pi''} : \underset{\sim}{\mathbf{R}}^{k(\pi')} = 0, \tag{28b}$$

while double sums of terms $\underset{\sim}{\mathbf{R}}^{g(\pi)} : \underset{\approx}{\mathbf{t}}'^{\pi''}_{C\pi''} : \underset{\sim}{\mathbf{R}}^{k(\pi')}$ or simple sums of terms $\underset{\sim}{\mathbf{R}}^{g(\pi)} : \underset{\approx}{\mathbf{t}}'^{\pi''}_{C\pi''}$ or $\underset{\approx}{\mathbf{t}}'^{\pi''}_{C\pi''} : \underset{\sim}{\mathbf{R}}^{k(\pi')}$ can collectively be cancelled for given groups of systems.

In the laminate frame, the laminate π is taken normal to the $x3$ axis. Then, the non-zero terms of the modified strain Green platelet operator $\underset{\approx}{\mathbf{t}}^{\pi}_{C\pi}$ are for $(i,j) \neq 1,2,6$, using the contracted 6×6 notation for four-rank symmetric tensors, i.e. (1, 2, 3, 4, 5, 6) = (11, 22, 33, 23, 31, 12). Correspondingly, the non-zero terms of its dual stress operator $\underset{\approx}{\mathbf{t}}'^{\pi}_{C\pi} = \underset{\approx}{C}^{\pi} - \underset{\approx}{\mathbf{C}}^{\pi} : \underset{\approx}{\mathbf{t}}^{\pi}_{C\pi} : \underset{\approx}{\mathbf{C}}^{\pi}$ which appears in the tensors $[\underset{\approx}{\mathbf{F}}]$ are for $(i,j) \neq 3,4,5$. In the operator $\underset{\approx}{\mathbf{t}}'^{\pi}_{C\pi}$, the elasticity moduli are expressed in the laminate frame. For general elasticity anisotropy, they can therefore have any elasticity symmetry depending on the laminate's crystallographic orientation within the crystal structure. For an identically oriented lattice frame in all platelet local frames, what is the case for all laminate orientations of same (*hkl*) crystallographic family, all the involved platelet operators $\underset{\approx}{\mathbf{t}}'^{\pi}_{C\pi}$ are identical, up to a rotation, and can be denoted $\underset{\approx}{\mathbf{t}}'^{\pi}$. This investigation is summarized in Appendix, addressing separately homogeneous and heterogeneous elasticity. It mainly shows that, whether or not the material elasticity is isotropic, the only laminate orientations, always ensured to exist, that fulfill the orthogonality property for some set of slip systems inde-

pendently on their current slip activity are either those parallel to a slip plane or those normal to a slip direction. This holds for respectively any group of coplanar systems in that plane or any group of collinear systems in that direction. Following the LEDs theory (Kulhmann-Wilsdorf, 2002), such laminate structures for slip that result from dislocation gliding can be viewed as dislocation "carpets" and dislocation "walls" respectively, both arrangements being identified as main dislocation arrays of lowest possible energy resulting from crystal slip activity.

These solutions for the orthogonality property that have the remarkable characteristic of being independent from the slip activity on the concerned slip planes, are consistent with global strain compatibility in the sense provided by the homogenization procedure. They are not necessarily consistent in terms of individual strain compatibility conditions between laminate layers that hold in general for particular slip combinations from the simultaneously involved systems (Freidin et al., 2002). Strain compatibility conditions between laminates have been thoroughly investigated for FCC crystals in Ortiz and Repetto (1999). They have shown that the $(1,1,w)$ slip planes, with $w = 0$, 1, 2, 3, and ∞ for the $(0\,0\,1)$ cube planes allow strain compatible laminate orientations between slip system pairs for particular combinations of octahedral slip activity.

It is noteworthy that the orthogonality property here discussed can also be fulfilled for particular combinations of slip that are neither parallel nor perpendicular to a given laminate orientation. Some of such combinations can be independent on the relative activities on the involved systems, as pointed in Appendix. But most of them depend on these relative activities. An example is reported in Appendix for octahedral multiple slip in laminates parallel to cube planes (which can become easy glide planes of FCC structures at high temperatures or in some FCC superalloys (Estevez et al., 1995)). Such particular solutions may remain stable in particular loading situations, as during low amplitude fatigue for example.

Laminates parallel to twinning planes or normal to a twinning direction will also provide increments of twinning shear without related TFA-due contribution to the overall current stiffness. But a partly twinned domain is no longer crystallographically homogeneous, although it may still be elastically isotropic. If the case of twinning is to be specifically addressed in papers to come, it is noteworthy that most of the forthcoming discussion on the description of the poly-crystal morphology within the TFA context is valid for both slip and twinning shear.

4. Poly-crystal stiffness resulting from the TFA–HML description

In Franciosi and Berbenni (2007), the RSL–TFA–HML modeling first introduced for heterogeneous intra-crystalline plasticity has been extended to poly-crystals, based on an analogy that was let to be justified through a physical interpretation. This analogy results from the polar decomposition of the modified Green operator integral for a grain-like inclusion whose discrete forms are identical to the operator of a multi-laminate structure. Here, we examine more closely the extension of the modeling to poly-crystals, in terms of its interpretation and of its relevancy. We first recall the pointed operator analogy and the formerly proposed extension of the modeling. We develop a physical interpretation and we examine the limits within which this interpretation makes sense. Then, we consider more closely the conditions that make the TFA contributions negligible compared to the physical hardening when the latter is allowed to

vary over several orders of magnitude as for example it does from large to ultra-fine or nanometric grains (here, "nanometric" stands for grain sizes of a few tens of nanometers). This yields to specify a description of the poly-crystal morphology that is able to realize the established conditions. The result is the modification of our former modeling into a graded RSL–TFA–HML modeling that makes the stiffness response of the poly-crystal grain size dependent. This graded form of the modeling is consistent with the proposed physical interpretation in which the characteristics of the grain boundary and sub-boundary orientation distribution predominates on the ones of the mean grain shape.

4.1. Discrete polar decomposition of the inter-granular influence operators

Whether plastic strain is pure slip or combines slip and twinning, a poly-crystal is here treated as an assemblage of crystalline domains where incremental plastic straining only results from slip, while twinning generates microstructural changes between successive loading steps in the form of nucleated volume fractions of new domain orientations. While such new domains are generally treated like ordinary grains for convenience, the introduction of the HML structures for slip in poly-crystals will partly recover their laminate nature as shown in the following.

According to Sections 3.4 and 3.5, for crystal domains I with P (crystallographically identical) slip planes, assuming homogeneous elasticity and in-plane isotropy for the laminates, the $P\times P$ intra-crystalline operators $-\langle \underset{\approx}{\mathbf{F}}^{\pi(I)\pi'(I)}\rangle = -f_{\pi'(I)}\langle \underset{\approx}{\underline{\mathbf{F}}}^{\pi(I)\pi'(I)}\rangle$ in $H0^{\text{TFA-HML}}$ from Eq. (18) take the form of the sum $\sum_{\pi''(I)}\langle \phi^{\pi(I)\pi'(I)}_{\pi''(I)}\rangle \underset{\approx}{\mathbf{t}}'^{\pi''(I)}$ for $\pi(I),\pi'(I)\in(1,P)$. The related intra-crystalline stiffness contributions read:

$$H0^{TFA-HML}=\sum_{\pi''(I)}\sum_{\pi(I),\pi'(I)}\left(\sum_{g(\pi(I)),k(\pi'(I))}\overline{P}0^{g(\pi(I))}\underset{\sim}{\mathbf{R}}^{g(\pi(I))}\otimes\underset{\sim}{\mathbf{R}}^{k(\pi'(I))}\overline{P}0^{k(\pi'(I))}\right)::\langle\phi^{\pi(I)\pi'(I)}_{\pi''(I)}\rangle\underset{\approx}{\mathbf{t}}'^{\pi''(I)}. \tag{29}$$

These contributions vanish if, $\forall I$, all the $P0^{g\pi}\langle\phi^{\pi''}_{\pi\pi'}\rangle P0^{k\pi'}$ coefficients (no sum over repeated indices) are zero for the cases where the tensor products $\underset{\sim}{\mathbf{R}}^{g(\pi)}:\underset{\approx}{\mathbf{t}}'^{\pi''}:\underset{\sim}{\mathbf{R}}^{k(\pi')}=(\underset{\sim}{\mathbf{R}}^{g(\pi)}\otimes\underset{\sim}{\mathbf{R}}^{k(\pi')})::\underset{\approx\approx}{\mathbf{t}}'^{\pi''}$ are not cancelled by the orthogonality property (i.e. zero coefficients for the tensor products in which $\pi\neq\pi'\neq\pi''$). This is nearly achieved in the defined HML structures for intra-crystalline slip since the cancelled TFA terms correspond to the slip planes of dominant incremental activity, i.e. those associated with the largest $P0^{g\pi}\langle\phi^{\pi''}_{\pi\pi'}\rangle P0^{k\pi'}$ coefficients. This remains true as well for shear contributions that result from twinning.

In comparison, the inter-granular influence operators $\underset{\approx}{\underline{\mathbf{F}}}^{IJ}$ present in the expression of $H0^{\text{TFA}}$ (Eq. (19)) depend on a unique operator $\underset{\approx}{\mathbf{t}}'^{G}$ that characterizes the common shape attributed to the grains, as $\underset{\approx}{\underline{\mathbf{F}}}^{IJ}=(1-\frac{\delta^{IJ}}{f_J})\underset{\approx}{\mathbf{t}}'^{G}$. Considering an ellipsoidal grain shape makes $\underset{\approx}{\mathbf{t}}'^{G}$ uniform over the grain volume (Eshelby, 1957). This operator $\underset{\approx}{\mathbf{t}}'^{G}$ can be decomposed into elementary operators as

$$\underset{\approx}{\mathbf{t}}'^{G}=\int_{\Omega}\Psi^{G}_{(\omega)}\underset{\approx}{\mathbf{t}}'^{P}(\omega)\mathrm{d}\omega, \tag{30a}$$

where $d\omega = \sin\theta d\theta\, d\phi$ runs over the unit sphere Ω in R^3, $\Psi^G_{(\omega)} \geqslant 0$ is a characteristic weight function[4] such that $\int_\Omega \Psi^G_{(\omega)} d\omega = 1$, and $\mathbf{t}'^P(\omega)$ is the laminate operator of ω-oriented normal in R^3 (Franciosi and Lormand, 2004). From this polar decomposition, we can immediately notice that the tensor products $(\underset{\sim}{\mathbf{R}}^{g(\pi(I))} \otimes \underset{\sim}{\mathbf{R}}^{k(\pi'(J))}) :: (\int_\Omega \Psi^G_{(\omega)} \underset{\approx}{\mathbf{t}}'^P(\omega) d\omega)$ partly vanish thanks to the orthogonality property discussed in Section 3.5. Thus, a straightforward extension of the HML scheme to poly-crystals is the replacement of the continuous decomposition of $\underset{\approx}{\mathbf{t}}'^G$ in the inter-granular operators $\underline{\underline{\mathbf{F}}}^{IJ}$ in Eq. (30a) by a discrete decomposition $\underset{\approx}{\mathbf{t}}'^{(G)}$ defined as

$$\underset{\approx}{\mathbf{t}}'^{(G)} = \frac{\sum_I f_I \sum_{\pi(I)} f_{\pi(I)} \Psi^G_{\pi(I)} \underset{\approx}{\mathbf{t}}'^{\pi(I)}}{\sum_I f_I \sum_{\pi(I)} f_{\pi(I)} \Psi^G_{\pi(I)}}. \tag{30b}$$

This discrete decomposition only involves platelets that are favorably oriented in terms of their contribution to the material overall stiffness, i.e. those of no stiffness contributions thanks to the orthogonality property. Physically, the "favorable platelets" for all crystallographic structures are those parallel to the slip planes (or to the twinning planes) of high activity in the aggregate, complemented with the platelets that are normal to the slip (or to the twinning) directions. As defined in Eq. (30b) and disregarding twinning, each platelet operator in $\underset{\approx}{\mathbf{t}}'^{(G)}$ is supposed to contribute in proportion to both the slip activity intensity on the associated slip plane and the grain's concentration which this slip plane belongs to. Furthermore, it remains dependent on the grain shape through the use of a discrete part of the grain shape characteristic weight function ($\Psi^G_{(\omega)}$). It is noteworthy that $\underset{\approx}{\mathbf{t}}'^{(G)}$ is by definition a weighted sum of all the laminate components that participate in the intra-crystalline heterogeneities, such that in first approximation these intra-crystalline contributions are also accounted for, in average manner, by $\underset{\approx}{\mathbf{t}}'^{(G)}$. Then, disregarding the terms that specifically represent the intra-crystalline heterogeneities recalled by Eq. (29), a one-level TFA–HML modeling for poly-crystals results only from substituting $\underset{\approx}{\mathbf{t}}'^{(G)}$ for $\underset{\approx}{\mathbf{t}}'^G$. This modification, which amounts to removing a part of $\underset{\approx}{\mathbf{t}}'^G$, has been conjectured in our previous work as resulting from a new way to describe the overall poly-crystal morphology, in terms of a HML structure rather than in terms of a granular aggregate. Actually, this way, in a classical TFA framework, appears to be more relevant than representing grains or sub-domains by ellipsoids. We next develop further on this tentative interpretation.

4.2. Tentative physical interpretation of the TFA–HML scheme for poly-crystals

In aggregates, although the grains are the most often approximated as ellipsoidal for calculation simplicity, they much likely look like convex polyhedrons. Furthermore, intra-crystalline sub-structures building up during plastic deformation result in cellular partitions which are more likely polyhedral than ellipsoidal as well. It must be here stressed that whereas $\underset{\approx}{\mathbf{t}}'^G$ is exactly the stress modified Green operator integral over a grain-representative ellipsoidal domain, the operator $\underset{\approx}{\mathbf{t}}'^{(G)}$ as defined in Eq. (30b) is not. In general, it is not either the mean modified Green operator integral over some other type of geometrical domain (G). However, $\underset{\approx}{\mathbf{t}}'^{(G)}$ do is, as defined, the exact operator of some

[4] In the peculiar case of a spherical grain: $\Psi^{\mathrm{SPHERE}}_{(\omega)} = 1/4\pi\ \forall\omega$.

hierarchical multi-laminate structure that is here assumed to well characterize the polycrystal current morphological microstructure. This is also true for $\underset{\approx}{\mathbf{t}}'^{G}$ in Eq. (30a) that, prior to being representative of a reference ellipsoidal grain, represents a heterogeneous – possibly HML – morphology of ellipsoidal overall symmetry.

This tentative interpretation for $\underset{\approx}{\mathbf{t}}'^{(G)}$, as the representative operator of some structure (G) described as a HML one, can be supported by statistical considerations: let (G) be a multi-phase material (the crystalline orientations), with all phases of same statistically homogeneous characteristics function denoted $X_{(G)}(\mathbf{r})$. The phase covariance at the origin of the covariance space reads by definition of the Radon inversion formula in this context (Franciosi and Lormand, 2004):

$$\begin{aligned}\mathrm{Cov}^{(G)}(\mathbf{r}_0=0)&=\lim_{\mathbf{r}_0\to 0}\left(\int_{R^3}X_{(G)}(\mathbf{r})X_{(G)}(\mathbf{r}+\mathbf{r}0)\mathrm{d}\mathbf{r}\right)=\int_{\mathbf{R}^3}X_{(G)}(\mathbf{r})X_{(G)}(\mathbf{r})\mathrm{d}\mathbf{r}\\&=\frac{1}{8\pi^2}\int_{\omega\in\Omega}\left(\int_{z(\omega)}\left(\frac{\partial s_{(G)}(z,\omega)}{\partial z}\right)^2\mathrm{d}z\right)\mathrm{d}\omega=v^{(G)}.\end{aligned}\tag{31}$$

In Eq. (31), $s_{(G)}(z,\omega)$ is the area of the section of (G) cut by the plane of equation $z=\boldsymbol{\omega}\cdot\mathbf{r}$ and $v^{(G)}$ is the volume of (G). Therefore, the shape characteristic for this structure (G) is the shape of its covariance iso-contours near the origin. From this shape (G), Eq. (30b) defines a mean weight function $\overline{\Psi}^{(G)}_{(\omega)}$ that also specifies a characteristic mean operator $\underset{\approx}{\bar{\mathbf{t}}}'^{(G)}$ for (G).

Taking each term of $\overline{\Psi}^{(G)}_{(\omega)}$ as a probability to meet a grain or sub-grain boundary normal to a $\boldsymbol{\omega}$ direction, this mean weight function is representative of some statistically defined anisotropy of the orientation distribution of grain or sub-grain boundary facets in the aggregate. Thus, it can also be the interpretation given to the weight function introduced in Eq. (30b).

In this interpretation of the TFA–HML association in the modeling, the fact that the selected elementary laminate operators in $\underset{\approx}{\mathbf{t}}'^{(G)}$ are only those parallel to slip (or twinning) planes in the structure, or normal to slip (or twinning) directions, corresponds to assuming that grain or sub-grain boundary facets are mostly dense crystallographic planes (i.e. generally at first the planes of easiest glide). For sub-boundaries, dislocation "carpets" and dislocation "walls" (Kulhmann-Wilsdorf, 2002) make reasonable this assumption of polyhedral cellular sub-structures for which the crystallography defines the orientations of facets. Furthermore, it is now well supported (Mishra et al., 2007) that large plastic straining makes gradually intra-granular cell boundaries gaining a grain boundary character and so becoming impenetrable to dislocations. About grain boundary crystallography, the very many recent experimental and theoretical studies concerning Coincidence Site Lattices or DSC-lattices[5] (Davies and Randle, 2002; Schuh et al., 2005; Couzinié et al., 2005), do not make this assumption unreasonable. Indeed, the most frequently encountered grain boundaries in FCC crystals are the so-called "twin boundaries", parallel to the (1 1 1) planes, which are also frequent in hexagonal crystals. Grain boundaries between two grains tend to step-wise align with such planes of low energy. But totally suppressing the unfavorably oriented platelets as done in Eq. (30b) is certainly excessive for many materials if not for all, according to the details of their morphology. It is probably often unnecessary as well, with regard to the goal of making the TFA-due stiffness negligible compared to the hardening one.

[5] "Displacement Shift Complete" or "Displacements which are Symmetry Conserving".

It is not in the present scope to enter grain or sub-grain boundary analyses. But it is noteworthy that grain size and shape have a strong influence on the boundary crystallography, especially for ultra-fine and nanometric grains where the motion of only a few atoms can noticeably modify interface geometry (Bording et al., 2003; Zhu et al., 2007). The smaller the grain size, the more rounded their boundaries and the fewer their sub-boundaries become. Therefore, for small grain sizes, favorable boundary facets with regard to the orthogonality property would be less predominant, what tends to restrict the validity of this proposed extension of the RSL–TFA–HML modeling to poly-crystals with coarse grains. These physically founded remarks and limitations bring us to develop some grain size dependent gradation of the initial extension of the modeling to poly-crystals, in order to also make it relevant down to ultra-fine grains. This is addressed next.

4.3. Grain size dependency through a graded form of the RSL–TFA–HML modeling

With regard to the physical hardening, the decomposition of the modulus $H0_{\Sigma}$ as $H0_{\Sigma} = H0^{(h,\phi)} + H0^{(\mathrm{RFR},\Phi)}$ in Eq. (18), yields:

$$H0^{(h,\phi)} = \sum_{I,J} \sum_{g(I),k(J)} \overline{P}0^{g(I)} \left(\underline{h}^{g(I)k(J)} \left(\frac{\tau^{g(I)}}{\tau_c^{g(I)}} \right) - \underline{\phi}^{g(I)k(J)} \right) \overline{P}0^{k(J)}$$

$$\approx \sum_{I,J} \sum_{g(I),k(J)} \overline{P}0^{g(I)} \left(\underline{h}^{g(I)k(J)} \left(\frac{\tau^{g(I)}}{\tau_c^{g(I)}} \right) \right) \overline{P}0^{k(J)}.$$

By setting $H0^{(h,\phi)} = \frac{\mu}{k}$, with $k > 1$, the TFA contributions would become negligible enough for $\frac{H0^{(\mathrm{RFR},\Phi)}}{\mu} \ll \frac{1}{k} < 1$. For metallic poly-crystals with grain size in the μm range, the physical hardening level is typically $\mu/300$, such that $k \approx 300 \gg 1$. In comparison with the usual TFA contributions that can reach the value of $\mu/3$, a reduction by more than three orders of magnitude of $H0^{(\mathrm{RFR},\Phi)}$ would be needed to make it negligible compared to μ/k. This is quite equivalent to cancel it, as $H0^{\mathrm{TFA-HML}}$ nearly does. In contrast, for poly-crystals with ultra-fine grains, whose hardening can reach a few tens of the elasticity moduli (Billard et al., 2005; Capolungo et al., 2007), the TFA contributions would not need to be reduced that much to become negligible. The exact knowledge of the relevant physical mechanisms (inherent to interfacial plasticity) at the origin of this high physical hardening in small crystals is not needed for our interpretation. It can suit with any description of the complex behavior of fine-grained metallic aggregates, whether it be a micromechanical approach (Jiang and Weng, 2004; Capolungo et al., 2007) or an atomistic modeling of grain boundaries (Warner et al., 2006; Spearot et al., 2007), provided a physical internal length scale being introduced to quantify grain size effects, as also used in different contexts (Franciosi et al., 1998; Berbenni et al., 2007a,b,c).

Let us consequently consider a modification of the TFA modeling where, rather than arbitrarily suppressing the unfavorable part of $\mathbf{t}'^{G}$ in terms of effective stiffness, this part can be more or less reduced according to realistic microstructural considerations on boundary orientation distributions that may in particular be grain size dependent. From setting $\underset{\approx}{\mathbf{t}}'^{(G)} = \int_{\Omega} \Psi_{(\omega)}^{(G)} \underset{\approx}{\mathbf{t}}'^{P}(\omega) \mathrm{d}\omega$ in Eq. (30b) with $\Psi_{(\omega)}^{(G)} = \frac{f_I f_{\pi(I)} \Psi^G_{\pi(I)}}{\sum_{I'} \sum_{\pi(I')} f_{I'} f_{\pi(I')} \Psi^G_{\pi(I')}}$ when $\omega = \pi(I)$ or equals zero otherwise, we introduce the "α-graded operator" $\underset{\approx}{\mathbf{t}}'^{\langle G \rangle}$ of the form:

$$\underset{\approx}{\mathbf{t}}'^{\langle G\rangle} = \frac{\int_\Omega (\Psi^G_{(\omega)} + \alpha(\Psi^{(G)}_{(\omega)} - \Psi^G_{(\omega)}))\underset{\approx}{\mathbf{t}}'^{P}(\omega)\mathrm{d}\omega}{\int_\Omega (\Psi^G_{(\omega)} + \alpha(\Psi^{(G)}_{(\omega)} - \Psi^G_{(\omega)}))\mathrm{d}\omega} = \int_\Omega (\alpha\Psi^{(G)}_{(\omega)} + (1-\alpha)\Psi^G_{(\omega)})\underset{\approx}{\mathbf{t}}'^{P}(\omega)\mathrm{d}\omega, \tag{32a}$$

where $0 \leqslant \alpha \leqslant 1$, what is simply:

$$\underset{\approx}{\mathbf{t}}'^{\langle G\rangle} = \underset{\approx}{\mathbf{t}}'^{G} + \alpha(\underset{\approx}{\mathbf{t}}'^{(G)} - \underset{\approx}{\mathbf{t}}'^{G}) = \alpha\underset{\approx}{\mathbf{t}}'^{(G)} + (1-\alpha)\underset{\approx}{\mathbf{t}}'^{G}. \tag{32b}$$

Thus, the so defined modulus $H0^{(\mathrm{RFR},\Phi)} = H0^{\mathrm{TFA\text{–}HML}(\alpha)}$ depends on the weight α given to the "favorable contribution" $(\underset{\approx}{\mathbf{t}}'^{(G)} - \underset{\approx}{\mathbf{t}}'^{G})$ in the operator $\underset{\approx}{\mathbf{t}}'^{\langle G\rangle}$ and varies with increasing α from the usual TFA framework with $\underset{\approx}{\mathbf{t}}'^{\langle G\rangle} = \underset{\approx}{\mathbf{t}}'^{G}$ (when $\alpha = 0$) to its TFA–HML modification with $\underset{\approx}{\mathbf{t}}'^{\langle G\rangle} = \underset{\approx}{\mathbf{t}}'^{(G)}$ (when $\alpha = 1$). As required, the situation of coarse grains with a large contribution of favorably oriented sub-boundaries is consistent with a high α value and justifies the TFA–HML association in the modeling that is necessary to nearly cancel the TFA-due over-stiffness when the physical hardening is low. Conversely, for fine and ultra-fine grains, a not totally suppressed TFA-due inter-granular accommodation (because of prohibited high α values in this case) remains nevertheless negligible enough compared to a high physical hardening. Regardless of the dependency of k and of α with the grain size, this α-graded form of the RSL–TFA–HML modeling is made consistent with the proposed "boundary-based" interpretation of the poly-crystal morphology description by $\underset{\approx}{\mathbf{t}}'^{\langle G\rangle}$ as introduced in Eqs. (32) for any grain size from coarse grains ($\alpha = 1$) down to the nanometric range ($\alpha \to 0$). The formerly introduced RSL–TFA–HML modeling that corresponds to $\alpha = 1$ is consistent with this interpretation for coarse grains. The next section reports some numerical illustrations.

5. Compared stiffness and hardening for TFA and TFA–HML modeling of poly-crystals

Here, we report some simple simulations as original illustrations to compare poly-crystalline stiffness estimates from the graded TFA–HML(α) modeling with $0 \leqslant \alpha \leqslant 1$, using the globally regularized Schmid law, Eq. (1), as plastic flow criterion. For sake of simplicity, we have considered aggregates of homogeneous and shape-invariant spherical domains or "grains", with only two non-coplanar slip systems in each grain ($N = P = 2$, $p = 1$) and no twinning. The number of grain orientations is limited to four, with respective grain volume fractions f_1, f_2, f_3, f_4. For each grain I, the two ($P! = 2$) permitted rank-one HML structures correspond to laminates that are parallel either to the primary or to the secondary slip plane. They correspond to the hierarchies $P|(S)_I$ and $S|(P)_I$ according to the notations in Section 3.1. From Eqs. (21), the occurrence probabilities read $p(\pi(I)) = f_{\pi(I)} = \frac{P0^{\pi(I)}}{P0^{1(I)}+P0^{2(I)}}$ for $\pi = (P,\ S) = (1,2)$. For spherical grains, we have $\underset{\approx}{\mathbf{t}}'^{G} = \underset{\approx}{\mathbf{t}}'^{\mathrm{SPH}} = \frac{1}{4\pi}\int_\Omega \underset{\approx}{\mathbf{t}}'^{\omega}\mathrm{d}\omega$ as explicated in Section 4.1 and following section 4.3, the operator $\underset{\approx}{\mathbf{t}}'^{\mathrm{SPH}}$ is replaced by the graded form $\underset{\approx}{\mathbf{t}}'^{\langle\mathrm{SPH}\rangle} = \underset{\approx}{\mathbf{t}}'^{\mathrm{SPH}} + \alpha(\underset{\approx}{\mathbf{t}}'^{(\mathrm{SPH})} - \underset{\approx}{\mathbf{t}}'^{\mathrm{SPH}})$ with $\underset{\approx}{\mathbf{t}}'^{(\mathrm{SPH})} = \sum_I f_I(f_{1(I)}\underset{\approx}{\mathbf{t}}'^{1(I)} + f_{2(I)}\underset{\approx}{\mathbf{t}}'^{2(I)})$ and $0 \leqslant \alpha \leqslant 1$. We consider crystal orientations such that for all of them (see Fig. 2) both slip planes contain the $x3$ axis while all the slip directions are in the $x1$–$x2$ plane. Fig. 3a reports the tensile stress–strain curves of single crystals with

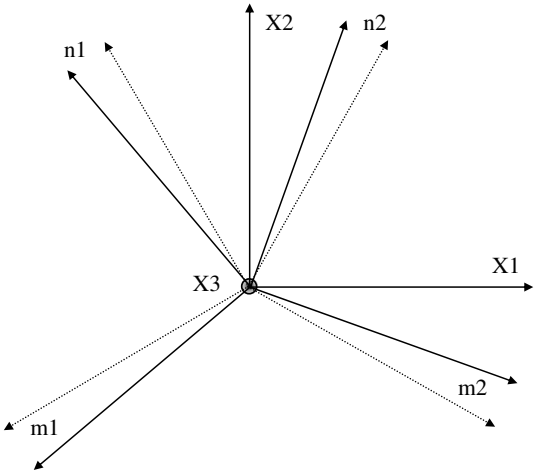

Fig. 2. Relative orientations of the two slip systems $(\mathbf{n}^1, \mathbf{m}^1)$ and $(\mathbf{n}^2, \mathbf{m}^2)$ in the pseudo crystals used for numerical simulations. The thin lines represent a second orientation of the same pseudo crystal. Both "single crystals" only rotate around the $x3$ axis that is normal to the figure plane.

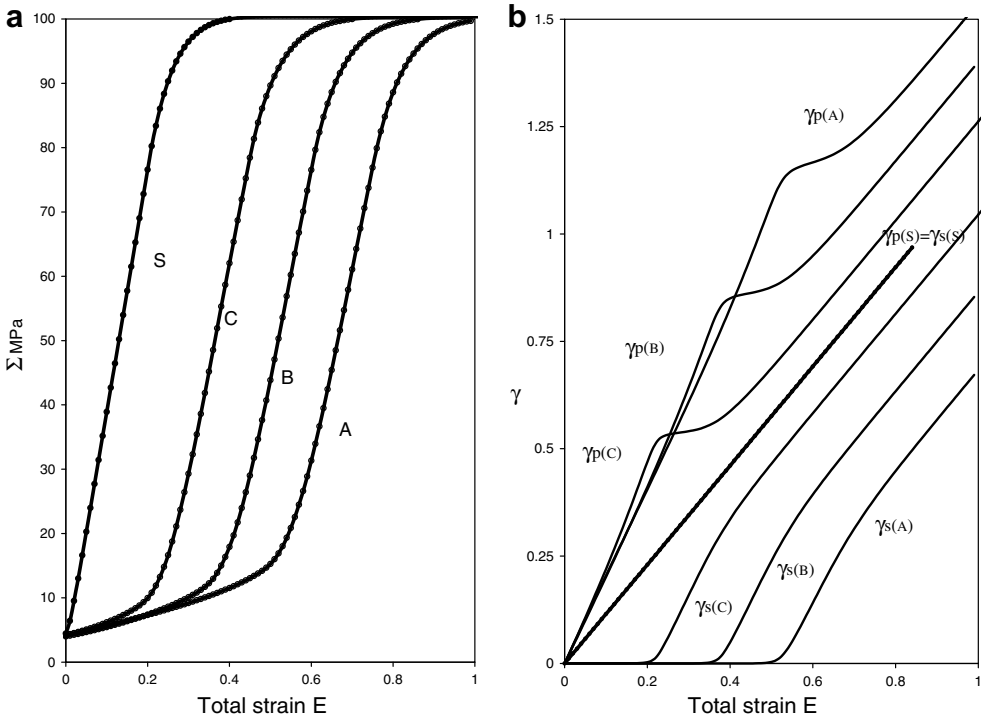

Fig. 3. (a) Stress–strain curves, (b) Primary and secondary slip, versus total strain for the A, B, C, S single crystals obeying the hardening law of Eq. (33) with hardening modulus $h0$ from Table 2 that corresponds to hardening range $\eta = 1$.

four different crystallographic orientations – denoted A, B, C, S – from which will be created the exemplified poly-crystals. The loading axis is $x1$ and the considered slip system orientations $\theta^{g(\alpha\,(\mathrm{I}))} = (x1, \mathbf{n}^{g(\alpha(\mathrm{I}))})$, $\phi^{g\,(\alpha(\mathrm{I}))} = (x1, \mathbf{m}^{g(\alpha(\mathrm{I}))})$, are listed in Table 1. The crystal S is a symmetric crystal with regard to its two slip systems. Crystal C is the closest to S and crystal A is the farthest. Tensile stress–strain curves are obtained either under the mixed loading conditions $\mathrm{d}E_{11} = d\varepsilon$, $\mathrm{d}\Sigma_{ij} = 0\ \forall ij \neq 11$, or, under the stress loading condition $\mathrm{d}\Sigma_{11} = \mathrm{d}\sigma$, $\mathrm{d}\Sigma_{ij} = 0\ \forall ij \neq 11$. For all grains, we have assumed a zero total rotation rate so that, with a non-zero plastic rotation rate around the $x3$ axis only, $\mathrm{d}\underset{\sim}{\omega}^{el}_{\alpha(I)} = -\mathrm{d}\underset{\sim}{\omega}^{pl}_{\alpha(I)} = (0, 0, (\mathrm{d}\gamma^{1(\alpha(I))} - \mathrm{d}\gamma^{2(\alpha(I))})/2)$. The crystallographic orientations are step-wise updated using the relations $\mathrm{d}\mathbf{n}^{g(\alpha(I))} = \mathrm{d}\underset{\sim}{\omega}^{el}_{\alpha(I)} \wedge \mathbf{n}^{g(\alpha(I))}$ (resp. $\mathrm{d}\mathbf{m}^{g(\alpha(\mathrm{I}))}$). The simulations make use of a realistic nonlinear and non-convex crystal hardening law taken in a local form as follows:

$$\mathrm{d}\tau^g_c = \sum_{k=1,2} h^{gk}\,\mathrm{d}\gamma^k = \sum_{k=1,2} 2h_0(1-R)\left[\frac{(a-(a-1)\delta^{gk}) + c\gamma^{\mathrm{Max}} + q(\Gamma - \gamma^{\mathrm{Max}})}{\tau^g_c + \tau^k_c}\right]\mathrm{d}\gamma^k \quad \text{for } g = 1,2, \tag{33}$$

with

$$\Gamma = \sum_k \gamma^k, \gamma^{\mathrm{Max}} = \max(\gamma^k), \quad R = \begin{cases} 0 & \text{for } \langle\tau_c\rangle < \tau_{0II}, \\ \left(\frac{\langle\tau_c\rangle - \tau_{0II}}{\tau_s - \tau_{0II}}\right) & \text{if } \langle\tau_c\rangle \in (\tau_{0II}, \tau_s). \end{cases} \tag{34}$$

Further assumptions on hardening parameters are $c \approx a$ and $q \gg a$. The coefficient $a > 1$ introduces an initial hardening anisotropy which decreases, first slowly during a stage I of single slip ($\Gamma = \gamma^{\mathrm{Max}} = \gamma$), then rapidly during a stage II where multiple slip operates ($\Gamma > \gamma^{\mathrm{Max}}$). Furthermore, the "recovery function" R gradually reduces the stage-II hardening according to a Voce-type law with a saturation shear stress τ_s, and, taking $\langle\tau_c\rangle = \sum_g f_g \tau^g_c$. In this analysis, we have disregarded late re-hardening stages, such as for example stage IV and subsequent ones in FCC crystals observed at large enough strains or high enough temperature (Franciosi, 1994; Mecif et al., 1997). The elasticity and hardening moduli values used in the simulations are reported in Table 2. The reference (Σ, E) curves of Fig. 3a exhibit for the crystals A, B and C the successive

Table 1
Orientations of the A, B, C, S pseudo single crystals that are used for the simulations

	$\theta(x1,n1)$	$\phi(x1,m1)$	$\theta(x1,n2)$	$\phi(x1,m2)$
Crystal A	0.8π	$0.8\pi + 0.5\pi$	0.4666666666π	$0.4666666666\pi - 0.5\pi$
Crystal B	$0.75 + \pi$	$0.75\pi + 0.5\pi$	0.4166666666π	$0.4166666666\pi - 0.5\pi$
Crystal C	0.7π	$0.7\pi + 0.5\pi$	0.3666666666π	$0.3666666666\pi - 0.5\pi$
Crystal S	$2\pi/3$	$2\pi/3 + 0.5\pi$	$\pi/3$	$\pi/3 - 0.5\pi$

Table 2
The elasticity and hardening parameters that are used for the simulations

Elasticity and yield	$\mu = 30$ GPa	$\nu = 0{,}3$	$\tau c0 = 2$ MPa	$\tau c0\mathrm{II} = 35$ MPa	$\tau\mathrm{s} = 45$ MPa
Hardening	$h0 = 2$	$A = 4$	$c = 2$	$q = 900$	$n = 20$

hardening stages I and II that are typically observed in FCC crystals for example. The slope of the stage I hardening that is observed on these curves well reproduces the experimental range of $\mu/10{,}000$. The farther the crystal orientation from the symmetric one S, the more important this hardening stage I is (Fig. 3a). In the case of the crystal S of symmetric orientation, the missing stage I (Fig. 3a) corresponds to stable equally double slip from the onset of plasticity. Fig. 3b displays the evolutions versus the tensile strain of the primary and secondary slip for the crystals A, B, C and S, respectively denoted "γp" and "γs". For the crystal S, equal double slip and no rotation yield a unique straight line. Applying Eq. (33) to the stage II ($R = 0$) and using the parameter values of Table 2 yields:

$$\tau_c^g = \tau_c^k = R^{g,k}\sigma = \sqrt{\tau_0^2 + 2h_0((1+a)\gamma + (c+q)\gamma^2)} \to \gamma\sqrt{2h_0(c+q)} \approx 60\gamma = \frac{\mu}{500}\gamma$$
$$= 10^{-3}\frac{\mu}{R^{g,k}}\varepsilon^p,$$

where the Schmid factors $R^{g,k}$ are equal to 0.448. This (asymptotic) value of $\mu/500$ for the stage II hardening modulus $\left(\sigma \approx \frac{\mu}{200}\varepsilon\right)$ is slightly lower than experimental data ranging around $\mu/300$. As discussed in Section 4.3, that corresponds to a physical hardening level $H0^{(h,\phi)} = \mu/k$, with $k \approx 500$. The recovery stage III appears slightly faster than the exper-

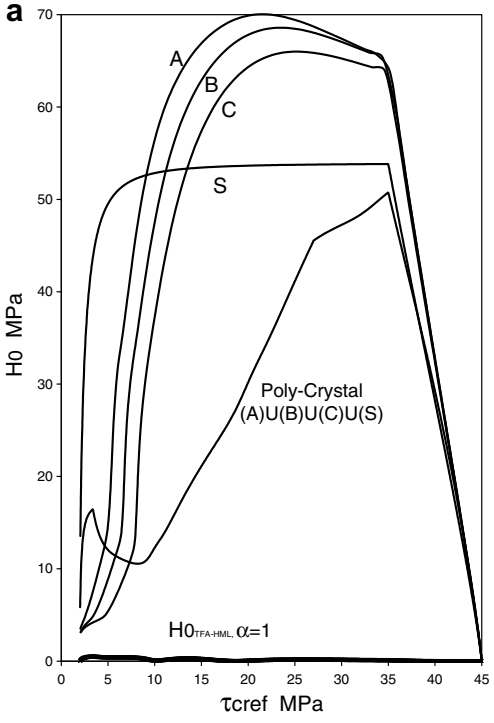

Fig. 4a. Hardening modulus $H0_\Sigma$ for the A, B, C, S single crystals and for the RSL–TFA–HML estimate ($\alpha = 1$) of the $A \cup B \cup C \cup S$ poly-crystal with its $H0^{\mathrm{TFA-HML}}$ part.

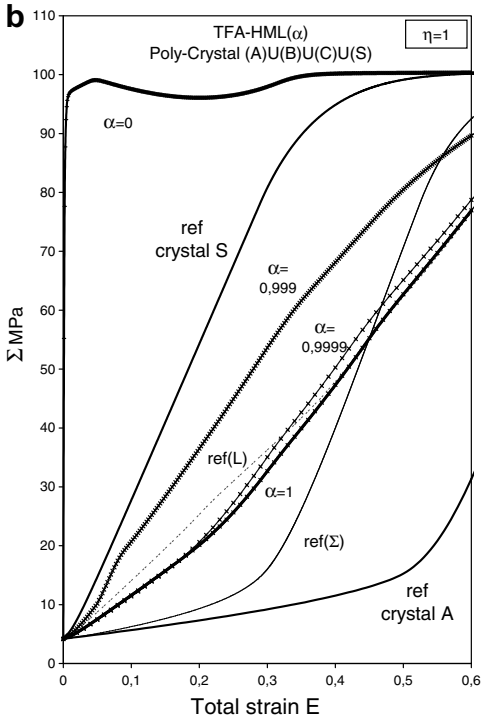

Fig. 4b. Stress–strain curves from the graded RSL–TFA–HML estimates for $0 \leqslant \alpha \leqslant 1$ of the A ∪ B ∪ C ∪ S poly-crystal, comparison with reference single crystals A and S and comparison with reference (L) and (Σ) estimates.

imentally observed ones. These minor discrepancies with experimental evidences do not induce any loss of generality for the reported observations.

The evolutions of the hardening modulus $H0_\Sigma = H0^{(h,\phi)} + H0^{(\mathrm{RFR},\Phi)}$ for the four crystals A, B, C, S along the successive hardening stages are plotted in Fig. 4a as a function of $\tau_{c\mathrm{ref}} = \langle \tau_c \rangle$. On this figure, we have also reported the RSL–TFA–HML(α) estimate of $H0_\Sigma$ when $\alpha = 1$ for the poly-crystal (A ∪ B ∪ C ∪ S) constituted of the four grain orientations with equal volume fractions $f_I = 0.25$. As also shown on Fig. 4a, the part of $H0_\Sigma$ due to $H0^{\mathrm{TFA-HML}(\alpha=1)} = H0^{(\mathrm{RFR},\Phi)}$ is clearly negligible. Fig. 4b compares the RSL–TFA–HML(α) estimates, for respectively $\alpha = 0$, $\alpha = 0.999$, $\alpha = 0.9999$ and $\alpha = 1$ ($0 \leqslant \alpha \leqslant 1$) that are obtained for the stress–strain curve of the poly-crystal (A ∪ B ∪ C ∪ S). On Fig. 4b, we have also reported the corresponding estimates arising from the assumptions of uniform stress and of uniform axial strain (respectively denoted "ref(Σ)" and "ref(L)") and we have recalled the reference curves of the single crystals S and A (from Fig. 3a). First, we can observe that the high TFA stiffness obtained when $\alpha \to 0$ makes the calculations unstable going towards the RSL–TFA modeling, but the relevant values of α for poly-crystals with coarse grains are close to 1.

For $\alpha = 1$, the RSL–TFA–HML estimate of the poly-crystal stiffness as shown in Fig. 4b is well in between the curves for the hardest S and the softest A single crystals, all along the successive hardening stages. Furthermore, it also remains in between the

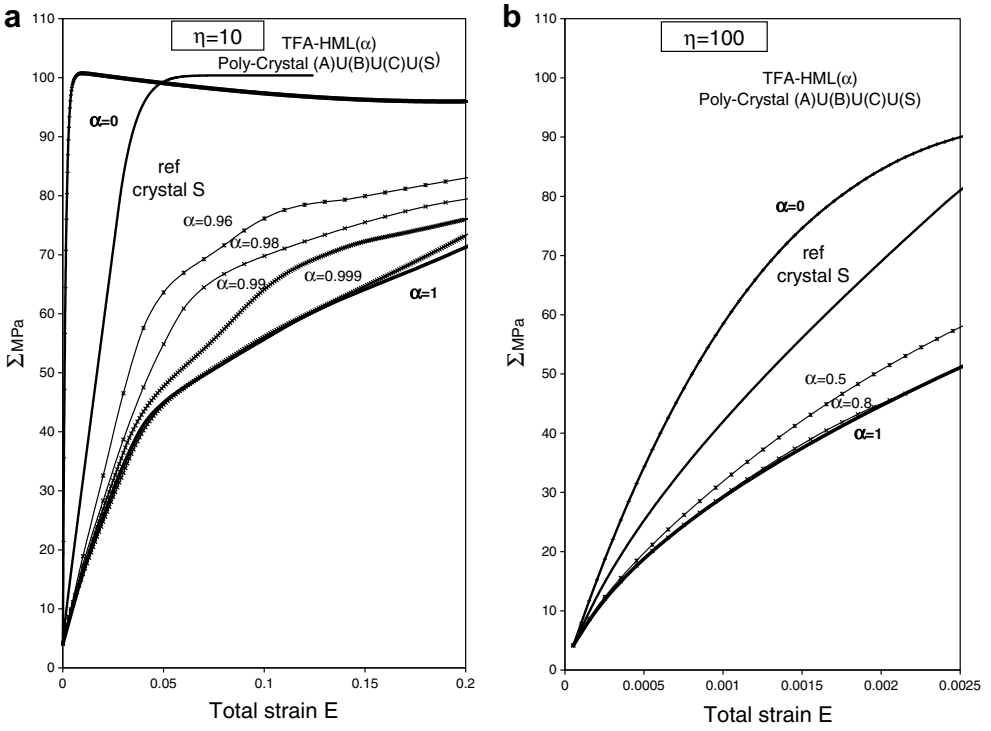

Fig. 5. Stress–strain curves for the S single crystal and from the graded RSL–TFA–HML estimates for $0 \leqslant \alpha \leqslant 1$ of the $A \cup B \cup C \cup S$ poly-crystal for hardening range (a) $\eta = 10$ and (b) $\eta = 100$.

ref(L) and ref(Σ) reference curves even when these ones cross each other.[6] For approximately $\alpha \in (1 - 10^{-5}, 1)$ there is no significant effect of the TFA-due stiffness compared to the predominant physical hardening term $H0^{(h,\phi)} \approx \mu/500$, and the results are convergent towards the curve obtained with $\alpha = 1$.

For $\alpha < 1 - 10^{-5}$, the effect of the TFA-due stiffness is no more negligible and it increases with decreasing α, as shown on Fig. 4b for $\alpha = 1 - 10^{-4} = 0.9999$ and for $\alpha = 1 - 10^{-3} = 0.999$. The RSL–TFA estimate ($\alpha = 0$) is much stiffer than the response of the hardest constitutive grain (S orientation). Theoretically, the RSL–TFA modeling is expected to predict a very high value of the modulus $H0^{\approx}_{\Sigma} H0^{(\mathrm{TFA})}$, of the range of $\mu/10$. According to the plotted curve (of slope $\approx \mu/3$) that is reported on Fig. 4a for a Schmid factor near 0.45, we can check that the obtained value for $H0^{\approx}_{\Sigma} H0^{(\mathrm{TFA})}$ is approximately $\mu/15$, what corresponds, for $k = 500$, to $\frac{H0^{(\mathrm{TFA})}}{H0^{(h,\phi)}} \approx \frac{100}{3}$. The α range of no TFA stiffness effect for that hardening value corresponds to $0 \leqslant 1 - \alpha < \frac{1}{10^5} \approx \frac{1}{200k}$, what means that the ratio $\frac{H0^{(\mathrm{TFA})}}{H0^{(h,\phi)}} \approx \frac{10^2}{3}$ needs to be reduced to $\frac{10^{-3}}{3}$ (i.e. more than three orders of magnitude as pointed in Section 4.3). Conversely, according to the hardening law form in Eq. (33), increasing the $H0^{(h,\phi)} = \mu/k$ modulus to the level of the $H0^{(\mathrm{TFA})} \approx \mu/15$ one, needs to multiply

[6] The TFA–HML estimate passes through the crossing point that is due to the non-convex hardening law of Eq. (33). The TFA–HML estimate closely follows the upper part of the ref(L) curve.

$H0^{(h,\phi)}$ by a factor $\eta = k/15$ and the h_0 modulus by η^2. For $k \approx 500$ that gives $\eta^2 \approx \left(\frac{10^2}{3}\right)^2 \approx 10^3$. Figs. 5a and b report several RSL–TFA–HML(α) estimates for $0 \leqslant \alpha \leqslant 1$, respectively for $\eta = 10 < \frac{10^2}{3}$ and $\eta = 100 > \frac{10^2}{3}$. The related reference curves for single crystal S are also reported. In a first approximation from these few comparisons, the α domain of no TFA effect that was $\alpha \in (1 - 10^{-5}, 1)$ for $\eta = 1$ becomes $\alpha \in (1 - 10^{-3}, 1)$ for $\eta = 10$ and $\alpha \in (1 - 10^{-1}, 1)$ for $\eta = 100$. It so appears a critical value $(1 - \alpha_c)$ that grossly scales with η^2, say with $(H0^{(h,\phi)})^2$, over which the TFA-due accommodation hardening is a negligible part of $H0_\Sigma$.

6. Conclusion

This work deals with the heterogeneous plastic deformation of crystals and poly-crystals that is modeled using a homogenization framework based on the transformation field analysis (TFA) and a globally regularized Schmid law (RSL) at the scale of the Homogeneous Equivalent Super-crystal. In Franciosi and Berbenni (2007), we have first shown that the TFA framework becomes more relevant by introducing a description of heterogeneous intra-crystalline slip activity in terms of hierarchical multi-laminate (HML) structures. We have demonstrated that this relevancy is due to an orthogonality property between influence operators and Schmid tensors in HML structures. This property makes most of the over-stiffness due to the TFA contributions to vanish when laminate layers are either parallel to slip planes or normal to slip directions. As treated by superposing all possible plastic strain modes of HML structure, the TFA–HML association is a particular case of non-uniform TFA (NTFA) modeling of the coupled type introduced by Michel and Suquet (2003, 2004). In the present paper, the extension of the RSL–TFA–HML modeling to poly-crystals that was previously introduced by analogy is examined in details and a physical interpretation is given. This extension amounts to describing the aggregate morphology from the orientation distribution of its boundary and sub-boundary facets rather than from its mean grain shape. In the proposed description, the favorable facet orientations that allow to lower the TFA accommodation hardening are those parallel to most active slip (or twinning) planes or normal to slip (or twinning) directions. The initial modeling extension to poly-crystals was therefore based on the strong assumption that all unfavorably oriented boundary and sub-boundary facets were absent. Since the larger the grain size, the larger the number of favorably oriented facets is (that includes sub-boundaries down to the cell structure scale), this strong assumption only holds for coarse grains. For ultra-fine grains, only a reduction of the contribution of the unfavorably oriented boundary facets is acceptable in this interpretation. But since the physical hardening in ultra-fine or nanometric grains is much higher, such a reduction is shown sufficient to still make the corresponding TFA accommodation negligible compared to the intra-crystalline hardening. Therefore, a graded form of the RSL–TFA–HML modeling has been proposed for poly-crystals that accounts for this grain size dependency of the effective stiffness in the context of the given interpretation. Simple applications to aggregates with realistic physical strain-hardening laws give successful results in terms of the stiffness estimates obtained from this graded RSL–TFA–HML modeling.

Appendix. Slip system orientations that fulfill the orthogonality property

A.1. Homogeneous elasticity (no twinning unless isotropy)

– When Eq. (28a) is expressed in the frame of the π laminate, it reads:

$$\underset{\sim}{\mathbf{t}}'^{\pi}_{C\pi} :: (\underset{\sim}{\mathbf{R}}^{g} \otimes \underset{\sim}{\mathbf{R}}^{k}) = t'_{11}\alpha^{gk}_{11} + t'_{12}\alpha^{gk}_{12} + t'_{16}\alpha^{gk}_{16} + t'_{22}\alpha^{gk}_{22} + t'_{26}\alpha^{gk}_{26} + t'_{66}\alpha^{gk}_{66} = 0, \tag{A1a}$$

with

$$\alpha^{gk}_{ii} = m^g_i n^g_i m^k_i n^k_i, \alpha^{gk}_{i6} = m^g_i n^g_i (m^k_1 n^k_2 + m^k_2 n^k_1) + (m^g_1 n^g_2 + m^g_2 n^g_1) m^k_i n^k_i \quad (i = 1, 2),$$
$$\alpha^{gk}_{66} = (m^g_1 n^g_2 + m^g_2 n^g_1)(m^k_1 n^k_2 + m^k_2 n^k_1)/2, \alpha^{gk}_{12} = m^g_1 n^g_1 m^k_2 n^k_2 + m^g_2 n^g_2 m^k_1 n^k_1.$$

The weakest elasticity symmetry corresponds to all six different and not necessarily zero t'_{ij} components for the laminate operator while the highest in-plane transversal isotropy (with regard to the $x3$ laminate axis) corresponds to only two different non-zero t'_{ij} components: $t'_{11} = t'_{22} = C_{11} - \frac{(C_{13})^2}{C_{33}}$ and $t'_{12} = t'_{21} = C_{12} - \frac{(C_{13})^2}{C_{33}}$ (with $t'_{66} = t'_{11} - t'_{12} = 2C_{66}$), such that Eq. (A1a) becomes $t'_{11}(\alpha^{gk}_{11} + \alpha^{gk}_{22} + \alpha^{gk}_{66}) + t'_{12}(\alpha^{gk}_{12} - \alpha^{gk}_{66}) = 0$. But any system pair (g,k) among the N^2 possible ones in the considered structure also satisfies the ten constraints $\mathbf{n}^g \cdot \mathbf{m}^g = 0$, $|\mathbf{n}^g| = |\mathbf{m}^g| = 1$ (resp. k) and $\mathbf{n}^g . n^k = a_i$, $\mathbf{n}^g \cdot \mathbf{m}^k = b_i$, $\mathbf{m}^g \cdot \mathbf{n}^k = c_i$, $\mathbf{m}^g \cdot \mathbf{m}^k = d_i$, $i \in (1, N^2)$. Solutions of Eq. (28a) that are not solution of Eq. (28b) exist, as for example any two vector pairs ($\mathbf{n}^g$, $\mathbf{m}^g$) and ($\mathbf{n}^k$, $\mathbf{m}^k$) that define orthogonal planes (G) and (K) both orthogonal to the laminate plane. Such vector pairs do not necessarily define two slip systems for the considered structure.[7] Admissible such solutions are expectedly more numerous in structures with more than two coplanar and/or collinear slip systems since for such groups a same plastic strain increment can be performed from contributions of a set of coplanar (resp. collinear) slip systems. But they do not always exist.

– When Eq. (28b) is expressed in the frame of the π laminate, it reads:

$$t'_{1i} m^g_1 n^g_1 + t'_{2i} m^g_2 n^g_2 + t'_{6i}(m^g_1 n^g_2 + m^g_2 n^g_1) = 0, \quad i = 1, 2, 6 \ (\text{resp} \cdot k). \tag{A1b}$$

The solutions fulfilling the three conditions of Eq. (A1b) for any elasticity symmetry applying on the three "free" components of the unit vectors ($\mathbf{n}^g$, $\mathbf{m}^g$) or ($\mathbf{n}^k$, $\mathbf{m}^k$) that also obey to $\mathbf{n}^g \cdot \mathbf{m}^g = 0$, $|\mathbf{n}^g| = |\mathbf{m}^g| = 1$ (resp.k), obviously correspond to one of the two involved Schmid tensors $\mathbf{R}^{g,k}$ of the form $(0, 0, 0, R^{g,k}_{23}, R^{g,k}_{31}, 0)$ in the laminate frame. That defines, whatever the considered crystal structure, a slip system g or k either with a slip plane parallel to the laminate ($\mathbf{n}^{g,k} = (0, 0, 1)$ and $\mathbf{m}^{g,k} = (m^{g,k}_1, m^{g,k}_2, 0)$) or with a slip direction normal to the laminate ($\mathbf{m}^{g,k} = (0, 0, 1)$ and $\mathbf{n}^{g,k} = (n^{g,k}_1, n^{g,k}_2, 0)$). In the case of the octahedral systems $(1\,1\,1)\langle 1\,1\,0\rangle$ of the FCC structure, these two laminate orientations correspond to the crystallographic planes $(1\,1\,1)$ and $(1\,1\,0)$. The same two types of laminate orientations result for BCC crystals when plastic strain is restricted to slip on systems $(1\,1\,0)\langle 1\,1\,1\rangle$, as well as for basal slip in HCP crystals. These types of solutions always exist.

– An example, in FCC crystals, of vanishing TFA-due over-stiffness for octahedral multiple slip in $(0\,0\,1)$ laminates. Regarding a $(0\,0\,1)$ plane, for equal double slip for example,

[7] Examples are in BCC crystals the slip systems $(1\,1\,2)\langle \bar{1}\,\bar{1}\,1\rangle$ and $(1\,\bar{1}\,2)\langle \bar{1}\,1\,1\rangle$ with regard to $(0\,0\,1)$-oriented laminates.

Eq. (23) reduces to a 2×2 ϕ weight matrix where $\phi^{i1} = -\phi^{i2}$, $i = 1,2$ from Eq. (26), such that slip system pairs with all equal coefficients make the TFA-due stiffness to globally vanish for a laminate orientation. For symmetry reason with regard to the (0 0 1) plane, the $N = 12$ FCC octahedral slip systems separate into two groups: group I of eight systems with slip direction at $\pi/4$ from the $x3 = \langle 0\,0\,1\rangle$ axis and group II of four systems with slip direction orthogonal to $x3 = \langle 001\rangle$. Considering the slip system $B4 = \langle \bar{1}01\rangle(1\,1\,1)$ in group I and $B5 = \langle 1\bar{1}0\rangle(1\,1\,1)$ in group II respectively as the reference system for the group, the computed four coefficients of Eq. (29a) in the cubic form $t'_{11}(\alpha^{gk}_{11} + \alpha^{gk}_{22}) + t'_{12}(\alpha^{gk}_{12}) + t'_{66}(\alpha^{gk}_{66}) = 0$ are collected for the 12 slip systems in Tables A1 and A2 where the Schmid and Boas notation is used (Tranchant et al., 1993). For cubic elasticity symmetry, system pairs (g,k) such that $\alpha^{gk}_{11} + \alpha^{gk}_{22} = \alpha^{gk}_{12} = \alpha^{gk}_{66} = 0$ do not show up. For transversally isotropic elasticity, system pairs (g,k) allowing $\alpha^{gk}_{11} + \alpha^{gk}_{22} + \alpha^{gk}_{66} = \alpha^{gk}_{12} - \alpha^{gk}_{66} = 0$, need $\frac{t'_{11}}{t'_{12}} = \frac{\lambda+2\mu}{\lambda} = \frac{\alpha^{gk}_{12} - \alpha^{gk}_{66}}{\alpha^{gk}_{11} + \alpha^{gk}_{22} + \alpha^{gk}_{66}} = 1 + \frac{1}{\nu}$ (or equivalently $\nu = -\frac{\alpha^{gk}_{11} + \alpha^{gk}_{22} + \alpha^{gk}_{66}}{\alpha^{gk}_{11} + \alpha^{gk}_{22} + \alpha^{gk}_{12}}$). Incompressible isotropic

Table A1
Equivalent octahedral slip systems of group 1 for FCC crystals and the parameter values involved in the orthogonality property (Eqs. (A1)) with regard to a $\langle 0\,0\,1\rangle$-oriented laminate

	m	n	α^{gk}_{11}	α^{gk}_{22}	α^{gk}_{12}	α^{gk}_{66}	S–B	ν
1	0, −1, 1	−1, 1, 1	0	0	1/6	−1/12	A2	1/2
2	1, 0, 1	−1, 1, 1	1/6	0	0	−1/12	A3	–
3	1, 1, 0	−1, 1, 1	1/6	0	−1/6	0	A6	–
4	0, −1, 1	1, 1, 1	0	0	1/6	1/12	B2	–
5(g)	**−1, 0, 1**	**1, 1, 1**	**1/6**	**0**	**0**	**1/12**	**B4**	–
6	1, −1, 0	1, 1, 1	−1/6	0	1/6	0	B5	–
7	0, 1, 1	−1, −1,1	0	0	1/6	1/12	C1	–
8	1, 0, 1	−1, −1,1	1/6	0	0	1/12	C3	–
9	1, −1, 0	−1, −1,1	1/6	0	−1/6	0	C5	–
10	0, 1, 1	1, −1, 1	0	0	1/6	−1/12	D1	1/2
11	−1, 0, 1	1, −1, 1	1/6	0	0	−1/12	D4	–
12	1, 1, 0	1, −1, 1	−1/6	0	1/6	0	D6	–

Typical multiple slip solutions, if any, include system no. 5 (B4) as system g.

Table A2
Equivalent octahedral slip systems of group 2 for FCC crystals and the parameter values involved in the orthogonality property (Eqs. (A1)) with regard to a $\langle 0\,0\,1\rangle$-oriented laminate

	m	n	α^{gk}_{11}	α^{gk}_{22}	α^{gk}_{12}	α^{gk}_{66}	S–B	ν
1	0, −1, 1	−1, 1, 1	0	1/6	−1/6	0	A2	–
2	1, 0, 1	−1, 1, 1	−1/6	0	−1/6	0	A3	–
3	1, 1, 0	−1, 1, 1	−1/6	−1/6	0	0	A6	0
4	0, −1, 1	1, 1, 1	0	1/6	−1/6	0	B2	–
5	−1, 0, 1	1, 1, 1	−1/6	0	−1/6	0	B4	–
6(g)	**1, −1, 0**	**1, 1, 1**	**1/6**	**1/6**	**0**	**0**	**B5**	**0**
7	0, 1, 1	−1, −1, 1	0	1/6	−1/6	0	C1	–
8	1, 0, 1	−1, −1, 1	−1/6	0	−1/6	0	C3	–
9	1, −1, 0	−1, −1, 1	−1/6	−1/6	0	0	C5	0
10	0, 1, 1	1, −1, 1	0	1/6	−1/6	0	D1	–
11	−1, 0, 1	1, −1, 1	−1/6	0	−1/6	0	D4	–
12	1, 1, 0	1, −1, 1	1/6	1/6	0	0	D6	0

Typical multiple slip solutions, if any, include system no. 6 (B5) as system g.

materials thus admit (B4, A2) and (B4, D1) pairs. Next, we consider the B4 reference system as active (Table A1) and we prospect for slip dependent solutions. For general elasticity anisotropy, equal slip on the (B4, C3) system pair is consistent with a globally vanishing TFA stiffness with a lamination orientation of (0 0 1) normal axis. So it is for multiple slip on larger system sets involving pairs of equally active systems such as (B2, C1), (A2, D1), (D4, A3), together with the (B4, C3) one (for example during axial-symmetric loading along the $\langle 0\,0\,1\rangle$ direction). For the B5 reference system assumed active (Table A2), equal slip on the (B5, D6) system pair, or multi-slip involving pairs of equally active systems such as (B5, D6) and (C5, A6) (resulting from some appropriate loading), would also be consistent with a globally vanishing TFA stiffness.

A.2. Heterogeneous elasticity

For sub-domains possibly of different lattice orientations, the number of situations to be considered in the homogeneous equivalent super-crystal is increased. The larger the number of elementary mechanisms, the larger the pairs or groups of mechanisms that may fulfill the orthogonality property for particular relative activities are. But according to the general form given by Eqs. (27) to the terms of the stress influence tensors, and thanks to the symmetry $\underset{\sim}{\mathbf{R}}^{g(\pi)} : (\underset{\approx}{\mathbf{B}}^{\pi}_{\pi''}) = (\underset{\approx}{\mathbf{B}}^{t\pi}_{\pi''}) : \underset{\sim}{\mathbf{R}}^{g(\pi)} = (\underset{\sim}{\mathbf{M}}^{g(\pi)}_{\pi''})$, Eqs. (27) can be written:

$$(\underset{\approx}{\mathbf{B}}^{t\pi}_{\pi''}) : \underset{\sim}{\mathbf{R}}^{g(\pi)} : \underset{\approx}{\mathbf{t}}'^{\pi''}_{C\pi''} : \underset{\sim}{\mathbf{R}}^{k(\pi')} : (\underset{\approx}{\mathbf{B}}^{\pi'}_{\pi''}) = 0, \tag{A2a}$$

$$(\underset{\approx}{\mathbf{B}}^{t\pi}_{\pi''}) : \underset{\sim}{\mathbf{R}}^{g(\pi)} : \underset{\approx}{\mathbf{t}}'^{\pi''}_{C\pi''} = 0 \quad \text{or} \quad \underset{\approx}{\mathbf{t}}'^{\pi''}_{C\pi''} : \underset{\sim}{\mathbf{R}}^{k(\pi')} : (\underset{\approx}{\mathbf{B}}^{\pi'}_{\pi''}) = 0. \tag{A2b}$$

If we focus our interest on solutions that do not depend on the relative slip or shear activities on the involved planes, the solution of Eq. (28b) are solutions of Eq. (A2a), (A2b). Same conditions will hold for twinning systems.

This can also be established from noticing that in the frame of a platelet π", the non-zero terms of the tensor $\underset{\approx}{\mathbf{H}}^{\pi}_{\pi''}$, which can be written $-\underset{\approx}{\mathbf{t}}'^{\pi''} : \underset{\approx}{\mathbf{B}}^{t\pi} = -\underset{\approx}{\mathbf{B}}^{\pi} : \underset{\approx}{\mathbf{t}}'^{\pi''}$ using Eq. (13a) are still those for which $(i,j) \neq 3,4,5$ (as for $\underset{\approx}{\mathbf{t}}'^{\pi''}_{C\pi''}$). Consequently, the form of $\underset{\approx}{\mathbf{H}}^{\pi}_{\pi''}$ still gives a zero product with $\mathbf{R}^{g(\pi)}$ in the cases when either $\mathbf{n}^{g(\pi)}$ or $\mathbf{m}^{g(\pi)}$ is in the laminate plane π". Thus, the conditions of Eqs. (27b), that can also be written $\underset{\sim}{\mathbf{M}}^{g(\pi)}_{\pi''} : \underset{\approx}{\mathbf{H}}^{\pi}_{\pi''} = \mathbf{R}^{g(\pi)} : (\underset{\approx}{\mathbf{B}}^{\pi}_{\pi''}) : \underset{\approx}{\mathbf{H}}^{\pi}_{\pi''} = 0$ or $\underset{\approx}{\mathbf{H}}^{\pi'}_{\pi''} : \underset{\sim}{\mathbf{M}}^{k(\pi')}_{\pi''} = \underset{\approx}{\mathbf{H}}^{\pi'}_{\pi''} : (\underset{\approx}{\mathbf{B}}^{t\pi'}_{\pi''}) : \mathbf{R}^{k(\pi')} = 0$, and by symmetry of $\underset{\sim}{\mathbf{M}}^{g(\pi)}_{\pi''}$, and/or of $\underset{\sim}{\mathbf{M}}^{k(\pi')}_{\pi''}$, as $\underset{\sim}{\mathbf{R}}^{g(\pi)} : \underset{\approx}{\mathbf{H}}^{\pi}_{\pi''} : (\underset{\approx}{\mathbf{B}}^{t\pi}_{\pi''}) = 0$ or $(\underset{\approx}{\mathbf{B}}^{\pi'}_{\pi''}) : \underset{\approx}{\mathbf{H}}^{\pi'}_{\pi''} : \underset{\sim}{\mathbf{R}}^{k(\pi')} = 0$, are fulfilled.

References

Arminjon, M., 1991. A regular form of the Schmid law, application to the ambiguity problem. Textures and Microstructures, 1121–1128.

Berbenni, S., Franciosi, P., 2004. Yield surfaces using an extension of the " Regularized" Schmid law to polycrystalline materials. In: Gutkowski, W., Kowalewski, T.A. (Eds.), Proceedings of the 21th International Congress of Theoretical and Applied Mechanics—IUTAM Symposium, 15–21 August 2004, Warsaw, Poland.

Berbenni, S., Favier, V., Berveiller, M., 2007a. Impact of the grain size distribution on the behaviour of heterogeneous materials. International Journal of Plasticity 23, 114–142.

Berbenni, S., Favier, V., Berveiller, M., 2007b. Micro–macro modelling of the effects of the grain size distribution on the plastic flow stress of heterogeneous materials. Computational Materials Science 39, 96–105.

Berbenni, S., Nicaise, N., Richeton, T., Berveiller, M., 2007c. On grain size dispersion effects in metallic polycrystals and internal lengths associated with discrete plastic slip heterogeneities. In: Proceedings of the

11th International Symposium on Continuum Models and Discrete Systems, 30 July–3 August 2007, Paris, France.

Berveiller, M., Muller, D., Kratochvil, J., 1993. Non local versus local elastoplastic behavior of heterogeneous materials. International Journal of Plasticity 9 (5), 633–652.

Billard, S., Fondère, J.P., Bacroix, B., Dirras, G.F., 2005. Macroscopic and microscopic aspect of the deformation and fracture mechanisms of ultrafine-grained aluminum processed by hot isostatic pressing. Acta Materialia 54, 411–421.

Bording, J.K., Li, B.Q., Shi, Y.F., Zuo, J.M., 2003. Size and shape-dependent energetics of nanoscale interfaces: experiment and simulation. Physical Review Letters 90 (22), 226104-1–226104-4.

Capolungo, L., Cherkaoui, M., Qu, J., 2007. On the elastic visco-plastic behavior of nanocrystalline materials. International Journal of Plasticity 23 (4), 561–591.

Chaboche, J.-L., Kruch, S., Maire, J.-F., Pottier, T., 2001. Towards a micromechanics based inelastic and damage modeling of composites. International Journal of Plasticity 17, 411–439.

Couzinié, J.P., Decamps, B., Priester, L., 2005. Interaction of dissociated lattice dislocation with a Σ3 grain boundary in copper. International Journal of Plasticity 21 (4), 759–775.

Darrieulat, M., Piot, D., 1996. A method of generating analytical yield surfaces of crystalline materials. International Journal of Plasticity 12 (5), 575–610.

Davies, H., Randle, V., 2002. Single-section plane assessment in grain boundary engineering brass. Journal of Microscopy 205, 253–258.

Debotton, G., Hariton, I., 2002. Rank-infinity laminated composites attaining the Hashin–Shtrikman bounds. Physics Letters A 297, 442–445.

Dvorak, G.J., 1992. Transformation field analysis in inelastic composite materials. Proceedings of the Royal Society of London A437, 311–327.

Dvorak, G.J., Benveniste, Y., 1992. On transformation strains and uniform fields in multiphase elastic media. Proceedings of the Royal Society of London A437, 291–310.

Dvorak, G.J., Bahei-El-Din, A., 1997. Inelastic composite materials: transformation field analysis and experiments. In: Suquet, P. (Ed.), Continuum Micromechanics, CISM Course and Lecture, 377. Springer Verlag, Berlin, pp. 1–59.

El Omri, A., Fennan, A., Sidoroff, F., Hihi, A., 2000. Elastic–plastic homogenization for layered composites. European Journal of Mechanics A/Solids 19, 585–601.

Estevez, R., Hoinard, G., Franciosi, P., 1995. Hardening anisotropy of γ/γ' superalloy single crystals Part II: numerical analysis of heterogeneity effects. Acta Metallurgica and Materialia 45 (4), 1567–1584.

Eshelby, J.D., 1957. The determination of the elastic field of an ellipsoidal inclusion and related problems. Proceedings of the Royal Society London A241, 376–396.

Francfort, G., Murat, F., 1986. Homogenization and optimal bounds in linear elasticity. Archive for Rational Mechanics and Analysis 94, 307–334.

Franciosi, P., 1988. On flow and work hardening expression correlations in metallic single crystal plasticity. Revue de Physique Appliquée 23, 383–394.

Franciosi, P., 1994. Introduction of equivalent deformation mechanisms for the description of FCC crystals post-stage II plasticity kinematics. Key Engineering Materials, 323–328.

Franciosi, P., Zaoui, A., 1991. Crystal hardening and the issue of uniqueness. International Journal of Plasticity 4, 295–311.

Franciosi, P., Lormand, G., 2004. Using the Radon transform method to solve inclusion problems in elasticity. International Journal of Solids and Structures 41 (3/4), 585–606.

Franciosi, P., Berbenni, S., 2007. Heterogeneous crystal and polycrystal plasticity modeling from transformation phase analysis within a regularized Schmid flow law. Journal of the Mechanics and Physics of Solids 55 (11), 2265–2299.

Franciosi, P., Tranchant, F., Vergnol, J., 1993. On the twinning initiation criterion in Cu–Al α single crystals. II: correlations between the micro structure characteristics and the twinning initiation. Acta Metallurgica and Materialia 41 (5), 1543–1553.

Franciosi, P., Lormand, G., Fougères, R., 1998. On elastic modelling of inclusion induced microplasticity in metallic matrices from the dilatating sphere problem. International Journal of Plasticity 14 (10–11), 1013–1032.

Freidin, A.B., Viltchevskaya, E.N., Sharipova, L.L., 2002. Two-phase deformations within the framework of phase transition zones. Theoretical and Applied Mechanics, 149–172.

Gambin, W., 1991. Plasticity of crystals with interacting slip systems. Engineering Transactions 39 (3/4), 303–324.

Gambin, W., 1992. Refined analysis of elastic plastic crystals. International Journal of Solids and Structures 29, 2013–2021.

Hill, R., 1965. Continuum micro-mechanics of elastoplastic poly-crystals. Journal of the Mechanics and Physics of Solids 13, 89–101.

Imbault, D., Arminjon, M., 1998. Deformation textures of fcc materials predicted with a regular form of the Schmid law. Materials Science Forum, 371–376.

Jiang, B., Weng, G.J., 2004. A theory of compressive yield strength of nano grained ceramics. International Journal of Plasticity 20, 2007–2026.

Kocks, U.F., Franciosi, P., Kawai, M., 1991. A forest model of latent hardening and its application to poly-crystal deformation. Textures and Microstructures, 1103–1114.

Kowalczyk, K., Gambin, W., 2004. Model of plastic anisotropy evolution with texture dependent yield surface. International Journal of Plasticity 20, 19–54.

Kulhmann-Wilsdorf, D., 2002. Why do dislocations assemble into interfaces in Epitaxy as well as in crystal plasticity? To minimize free energy. Metallurgical and Materials Transactions A 33 (8/1), 2519–2539.

Masson, R., Bornert, M., Suquet, P., Zaoui, A., 2000. An affine formulation for the prediction of the effective properties of non linear composites and poly-crystals. Journal of the Mechanics and Physics of Solids 48 (6/7), 1203–1227.

Mc Ginty, R.D., Mc Dowell, D.L., 2006. A semi-implicit integration scheme for rate-independent finite crystal plasticity. International Journal of Plasticity 22 (6), 996–1025.

Mecif, A., Bacroix, B., Franciosi, P., 1997. Temperature and orientation dependent plasticity features of Cu and Al single crystals under axial compression. Acta Materialia 45 (1), 371–381.

Michel, J.C., Suquet, P., 2003. Non uniform transformation field analysis. International Journal of Solids and Structures 40, 6937–6955.

Michel, J.C., Suquet, P., 2004. Computational analysis of nonlinear composite structures using the nonuniform transformation field analysis. Computer Methods in Applied Mechanics and Engineering 193, 5477–5502.

Mishra, A., Kad, B.K., Gregori, F., Meyers, M.A., 2007. Microstructural evolution in copper subjected to severe plastic deformation: experiments and analysis. Acta Materialia 55, 13–28.

Ortiz, M., Repetto, E.A., 1999. Non convex energy minimization and dislocation structures in ductile single crystals. Journal of the Mechanics and Physics of Solids 47, 397–462.

Ponte-Castaneda, P., Suquet, P., 1998. Non linear composites. Advances in Applied Mechanics 34, 172–302.

Quintanilla, J., Torquato, S., 1996. Microstructure and conductivity of hierarchical laminate composites. Physical Review E 53 (5), 4368–4378.

Salem, A.A., Kalidindi, S.R., Semiatin, S.L., 2005. Strain hardening due to deformation twinning in α-titanium: constitutive relations and crystal plasticity modeling. Acta Materialia 53, 3495–3502.

Schuh, C.A., Kumar, M., King, W.E., 2005. Universal features of grain boundary networks in FCC materials. Journal of Materials Science 40 (4), 847–852.

Spearot, D.E., Jacob, K.I., McDowell, D.L., 2007. Dislocation nucleation from bicrystal interfaces with dissociated structure. International Journal of Plasticity 23 (1), 143–160.

Suquet, P., 1997. Effective behavior of non linear composites. In: Suquet, P. (Ed.), Continuum Micromechanics, CISM Course and Lecture, 377. Springer Verlag, Berlin, pp. 220–259.

Tranchant, F., Vergnol, J., Franciosi, P., 1993. On the twinning initiation criterion in Cu–Al α single crystals 1. Experimental and numerical analysis of slip and dislocation patterns up to the onset of twinning. Acta Metallurgica and Materialia 41 (5), 1532–1541.

Warner, D.H., Sansoz, F., Molinari, J.F., 2006. Atomistic based continuum investigation of plastic deformation in nanocrystalline copper. International Journal of Plasticity 22 (4), 754–774.

Zhu, T., Li, J., Samanta, A., Hyung, G.K., Suresh, S., 2007. Interfacial plasticity governs strain rate sensitivity and ductility in nanostructured materials. Proceedings of the National Academy of Science, USA 104 (9), 3031–3036.